Investigation of Lipid-PEG Anchorage of Proteins onto Mesenchymal Stem Cell Derived Extracellular Vesicles for Intracellular Delivery: A Quantitative Assessment

Antonin Marquant[1], Jade Berthelot[1], Claudia Bich[2], Zeineb Ibn Elfekih[1], Laurianne Simon[1], Baptiste Robin[1], Joël Chopineau[1], David Tianpei Wang[3], Samuel Jay Emerson[3], Aijun Wang[3], Clément Benedetti[4], Simon Langlois[4], Laurence Guglielmi[5], Pierre Martineau[5], Anne Aubert-Pouëssel[1] and Marie Morille[1,6*]

[1] ICGM, Montpellier University, CNRS, ENSCM, Montpellier, France.

[2]Institut des Biomolécules Max Mousseron (IBMM), UMR 5247-CNRS-UM-ENSCM, Montpellier, France.

[3]Center for Surgical Bioengineering, University of California Davis, Sacramento, California, USA.

[4]Montpellier Ressources Imagerie, BioCampus, University of Montpellier, CNRS, INSERM, Montpellier, France.

[5]Institut de Recherche en Cancérologie de Montpellier (IRCM), INSERM U1194, Montpellier, France.

[6]Institut universitaire de France (IUF), Paris, France.

*Corresponding author

Abstract

Extracellular Vesicles (EVs) are promising natural therapeutic vectors for delivery of cargos. However, loading of proteins into/onto EVs remains a major challenge limiting their interest as protein delivery system. Major hurdles are low loading efficiency and lack of absolute metrics regarding protein loading and cellular uptake. Here, interest of Lipid-PEG anchorage to trigger cargo protein association to murine mesenchymal stem cells derived EVs for intracellular delivery was investigated. HRP was used as a functional model protein to focus this study on absolute quantitative metrics. Impact of different structural parameters such as lipid anchor nature (cholesterol and DSPE), PEG linker molecular weight (MW) and physical parameters (temperature, cargo concentration) were studied. In contrast to native HRP, Lipid-PEG-HRP was significantly and stably associated to EVs and intracellularly delivered. Cholesterol anchor allowed an association of ≈1000 HRP per EVs which was 3.5-folds higher than DSPE, while highest MW PEG linker impacted cell internalization by steric hindrance. Control of the HRP per EV ratio yielded to an efficient cellular uptake in three carcinoma cell lines (PANC-1, A549 and SKBR3 cells). By thoroughly characterizing Lipid-PEG-protein anchorage, this study evidences the compatibility of this approach for EV protein delivery in addition to provide useful metrics.

Keywords

Exosomes, EV exogenous engineering, Cell delivery, Protein anchorage, Polymers, Click-chemistry

Graphical abstract

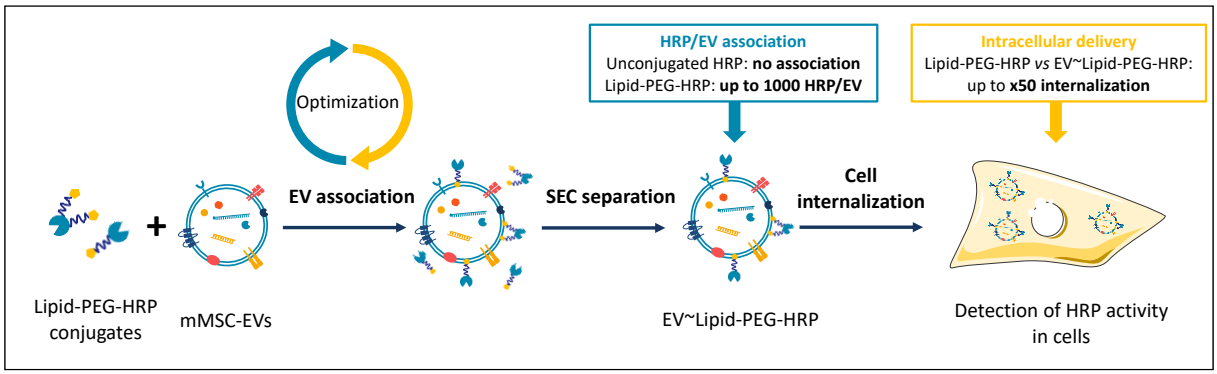

1. Introduction

Therapeutic proteins are powerful and fast-acting drugs that have proved their efficacy for many years in the treatment of a wide range of pathologies such as cancers[1–3], infectious or genetic diseases (HIV infection[4], cystic fibrosis[5], etc.) or auto-immune pathologies[6,7]. By contrast to small molecules, proteins have pharmacological effects at very low concentration and are able to be highly specific for their targets[8] (e.g., antibodies or enzymes towards their epitope or substrate). Therefore, these biomolecules are the best candidates for the interference of complex Protein-Protein Interactions (PPI) often implied in hard-to-drug pathologies. As a consequence, development of therapeutic proteins has soared over the two last decades leading proteins such as antibodies to be now top-tier drugs[9] and this trend is expected to continue[10]. However, despite their very interesting intrinsic properties, proteins also struggle with important limitations hindering their therapeutic potential. Delivery is one of the main challenges to overcome, as these fragile macromolecules face numerous barriers before reaching their target, especially if intracellular delivery is sought. In this case, proteins have to cross the cell membrane before escaping from endosomes to avoid lysosomal degradation and finally reach the molecular target (antigen for example)[11,12]. However, crossing cell membrane is almost impossible for these large and complex molecules. As a result, most of currently marketed therapeutic proteins target extracellular sites such as membrane proteins[13] whereas the ability to interfere with deleterious intracellular processes could lead to highly effective therapeutic options.

As a consequence, different approaches have been investigated to allow protein cytoplasmic delivery. One of the most straightforward and oldest strategy consists in direct physical transfer into the target cell. Predominantly exploited methods include electroporation and microinjection which are more dedicated to *in vitro* use[14]. In parallel, more suitable alternative solutions for *in vivo* administration have been developed such as protein engineering (e.g., lipidation, fusion with supercharged proteins or peptides)[10] or nanoparticle-based delivery using inorganic or organic nanocarriers[12] and finally, more recently natural nanoparticles such as Extracellular Vesicles (EVs)[15]. EVs are produced by the totality of known cells and organisms and have the ability to vectorize biomolecules from nucleic acids to proteins, making them a highly attractive alternative to synthetic nanoparticle-based therapies[16]. EVs have been successfully used to deliver proteins such as enzymes (cytosine deaminase[17], TPP1[18], Cre recombinase[19,20], Cas9 endonuclease[21,22], etc.) and various other proteins (SARS-CoV-2 spike protein[23], etc.) relying on endogenous (e.g., using cell engineering for protein fusion[19,24–26] or lipid anchorage signal[27–29]) or exogenous (using isolated EV, for instance with membrane permeabilization approach[18,30]) loading methods[15]. However, comparison between all of these approaches is difficult due to the lack of reported metrics, especially about loading/association

capacity (cargo per EV) and delivery (amount of cell-internalized cargo). Using endogenous approaches, the engineering efficiency (i.e., the proportion of EV loaded as compared to total EV population) is generally below 30%[24,31–33] and restricted to certain subpopulations (i.e., depending on the EV marker protein selected), with a protein loading capacity in the range of 200 proteins/EV[24].

In this context, the use of Lipid Anchor (LA) conjugated to cargo is an appealing option to increase EV loading by exploiting hydrophobic interactions with the phospholipid EV membrane. Moreover, this strategy can be seen as more versatile, especially compared to fusion with EV proteins, because all EV sub-populations are enclosed by hydrophobic membrane. This approach has been successfully used with numerous cargos such as small chemicals[34,35], nucleic acids[36–40] and fluorophores[41,42]. Surprisingly, very few protein cargos were reported, maybe because these complex biomolecules are difficult to handle. Using DMPE-PEG_{2000}, anti-EGFR nanobodies were associated to EVs to enable specific targeting of tumoral cells[43]. Similarly, a COVID-19 vaccine was obtained by conjugating SARS-CoV-2 receptor-binding domain to EVs[23] using DSPE-PEG_{2000}. However, the aim of these studies was to decorate EVs for cell targeting or to elicit immune system response, but not to deliver a bioactive protein into cells. For this reason, few absolute metrics were provided, especially about the cellular uptake. Moreover, some fundamental parameters of LA-protein / EV association remain to be investigated, such as side-by-side comparison of the impact of the lipid nature and PEG linker Molecular Weight (MW). Consequently, there is currently a strong lack of information about the interest of this approach for protein delivery, despite being promising since this non-covalent interaction should promote the release and activity of the cargo protein from EVs after cell internalization. Indeed, both diffusion of the protein into the cytoplasm and its interaction with its target could be impeded by steric hindrance if the protein remains covalently associated to EV after internalization.

This study intends to demonstrate the feasibility, versatility and relevance of lipid anchoring of a cargo protein to EVs for cellular delivery. Horse Radish Peroxidase (HRP) was selected as a model protein to provide absolute quantitative metrics about both association and delivery in order to characterize this method. The aim was to exclude artifacts such as protein aggregates or degraded cargo from these readouts by following HRP activity instead of fluorescent labels. Michael-addition reaction between maleimide and thiol has been used to conjugate HRP with Lipid-PEG anchor prior to association of Lipid-PEG-HRP conjugates with EVs. Using both bulk and single particle analysis, influence of the lipid anchor nature (1,2-Distearoyl-sn-glycero-3-phosphoethanolamine (DSPE) or cholesterol (CLS)) was evaluated, as well as the molecular weight (MW) impact of the polyethylene glycol (PEG) linker (1000, 2000 and 5000g/mol) on HRP / EV association and subsequent cell internalization. The nature of the lipid anchor was identified as a key factor governing this association,

in contrast to PEG linker MW. However, PEG MW was shown to significantly impact cell internalization. Interestingly, Lipid-PEG-HRP / EV association showed a better stability than generally reported with smaller cargo. Altogether, this EV anchorage-based approach enables to finely control the number of enzymatically active HRP associated per EV (with an association capacity in the range of ≈1000 HRP/EV, depending on the EV type and LA) in order to achieve efficient intracellular delivery of an active enzyme. This strategy could therefore be an interesting option for the treatment of diseases requiring the intracellular delivery of a protein.

2. Results

2.1. Characterization and tunability of the association of Lipid-PEG-HRP conjugates to EVs

2.1.1 HRP concentration and temperature are key parameters for controlling the association of Lipid-PEG-HRP with EVs.

EVs produced from murine mesenchymal stem cells (mMSC) either from Everzom company (abbreviated as mMSC-EV#1) or produced in our laboratory (abbreviated as mMSC-EV#2) were characterized. These EVs exhibited mode size of 100±3nm and 99±4nm, respectively (Figure 1A). Particle/protein ratios were $9.10^8 \pm 8.10^7$ and $7.10^8 \pm 9.10^7$ particles per µg of protein respectively, assessed by µBCA using Bovine Serum Albumin (BSA) as reference and NanoTracking Analysis (NTA) for particle quantification (Figure 1A&B). Surface antigen profiles of mMSC-EV#1 and mMSC-EV#2 were then evaluated using a multiplex bead-based flow cytometric assay (MACPlex, Figure 1C). Similar patterns were observed for both EV sources and 13 significantly different signals out of the 37 tested were found. The presence of EV tetraspanins (CD9, CD81, CD63) corresponding to already described MSC-derived EVs patterns[44] was detected. Moreover, both EV samples were observed using Transmission Electron CryoMicroscopy (cryoTEM, Figure 1D) and contained expected bilayer vesicles. mMSC-EV#2 seemed to include slightly more multi-vesicular particles. Finally, super-resolution microscopy showed different relative expression of tetraspanins (Figure 1E). The three main cluster-types of mMSC-EV#1 were CD63+ (41±16%), CD9/CD63++ double positive (22±7%) and CD81+ (14±15%) and only 7±2% of clusters were CD9/CD63/CD81+++ triple positive. In contrast, 72±6% of mMSC-EV#2 were triple positive and 12±2% were CD9/CD63++ double positive.

Lipid-PEG-HRP (namely DSPE-PEG_{1000}-HRP, DSPE-PEG_{2000}-HRP, DSPE-PEG_{5000}-HRP and CLS-PEG_{2000}-HRP) were obtained after reaction of maleimide-functionalized HRP (mal-HRP) and Lipid-PEG-SH anchors as described in section 5.3.1 and summarized in Supplementary Figure 1B. Lipid-PEG-HRP conjugates were characterized by HPLC-MS (Supplementary Figure 1C). Conservation of enzymatic activity of HRP was controlled after conjugation (Supplementary Figure 1D).

A.

Characteristics	EV#1	EV#2
Producing cells	C3H/10T1/2 mMSC	Bone Marrow-mMSC
Production conditions	3D + shear stress (Everzom)	2D culture
EV enrichment method	TFF + SEC	UC
Protein/Particle ratio (µg/1.10^{10}EVs)	9.10^{8}±8.10^{7}	7.10^{8}±9.10^{7}
Mode (nm)	100±3	99±4
Standard Deviation (nm)	68±1	51±3

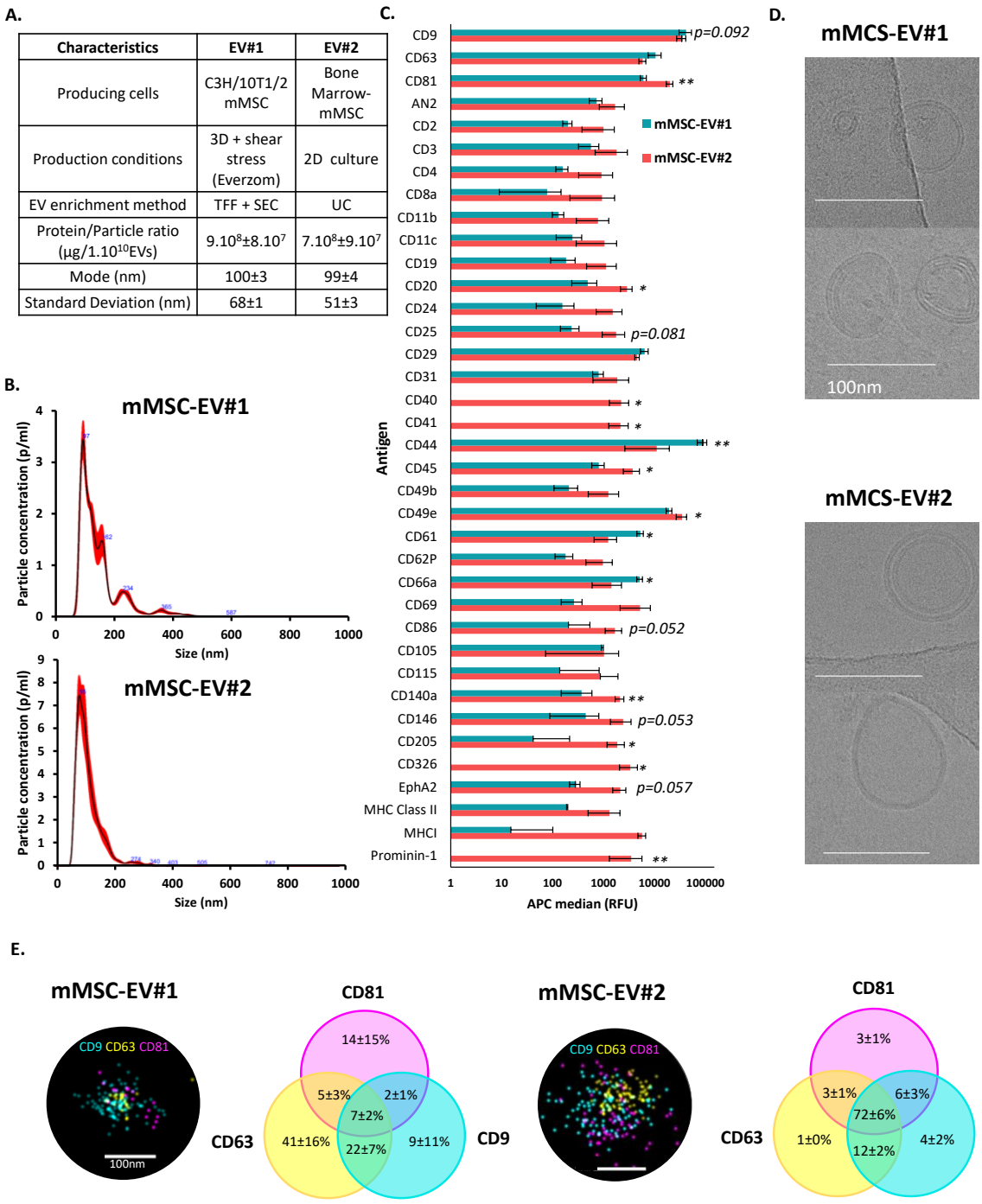

FIGURE 1 Characteristics of mMSC-EVs. (A) Production and enrichment characteristics. Protein full content was measured using µBCA assay and BSA as reference (n=3). EV concentration, mode and SD were measured using NTA (NS300). **(B)** Size distribution profiles measured by NS300. **(C)** MACSPlex Assay signal as APC median after subtraction of buffer background signal. MACSPlex triplicate on 3 different measurements for commercial mMSC-EV#1 and 3 different batches for mMSC-EV#2. MHCI, CD326, CD115, CD41, CD40 and CD20 were removed from mMSC-EV#1 due to high variability. **(D)** CryoTEM images of mMSC-EV#1 and #2. **(E)** Proportion of single, double and triple positive clusters of mMSC-EV#1 and #2 analyzed using super-resolution microscopy analysis. Samples were incubated with anti-CD9, -CD63 and –CD81 antibodies. Representative images of triple positive clusters are shown. Bar scale is 100nm (n=3). p-values were calculated using a two-tailed Welch test and are only indicated for p-value<0,10. *n.s*>0.05, *<0.05, **<0.01.

As a first step, SEC elution profiles of a fixed amount of native EVs (5.10^9 EV/ml) or protein (1µg/ml) were investigated using sepharose CL-2B to ensure that free HRP could be eluted separately from EVs using this method (Figure 2A). Fractions 3, 4 and 5 were identified as EV containing fractions (respectively 13±3%, 28±4%, and 16±2% relative to the initial quantity of EV loaded into the column) while retained free biologically active HRP in these fractions was respectively 0%, 0% and 2±1.4% before being mainly eluted in following fractions (F6-F10). Regarding this elution profile, F4 was selected to measure thoroughly the absolute association capacity, defined as the number of associated HRP per EV. When specified, F3, F4 and F5 fractions were pooled if a larger quantity of EVs was needed. To ensure that the retention of HRP with EVs in SEC fractions was the result of their association and not an artifact due to HRP and Lipid-PEG aggregates, three negative controls were added in association experiments: unconjugated HRP, Lipid-PEG-HRP alone (without EVs) and Lipid-PEG-CH_3 + HRP with EVs. For this last condition, the N-terminal methoxy function (CH_3) does not allow the covalent attachment of Lipid-PEG to mal-HRP. This control intended to identify the potential presence of free residual Lipid-PEG or Lipid-PEG micelles which may favor the formation of Lipid-PEG / HRP aggregates which could be co-separated and confused with EVs. Similarly, unconjugated HRP was the same mal-HRP than the one used for conjugation with Lipid-PEG (maleimide-modified HRP, obtained using sulfo-SMCC to conjugate maleimide functions on lysines) but not incubated with Lipid-PEG-SH. Potential unreacted HRP maleimide functions were expected to be hydrolyzed during the 24-hour dialysis step if not conjugated with Lipid-PEG-SH. Consequently, this control aimed at verifying that EV / HRP association was indeed due to the Lipid-PEG conjugation and not to an artifactual reaction between remaining maleimide functions of mal-HRP and cysteines of EV surface proteins.

Following this workflow, the influence of HRP concentration and incubation temperature was studied to identify optimal association conditions. First experiment set was done with a fixed EV concentration (5.10^{10} EV/ml) incubated with various concentrations of DSPE-PEG_{2000}-HRP (from 0.5µg/ml to 75µg/ml) at 25°C (Figure 2B). After SEC separation, association capacity was calculated based on the assumption of a homogeneous distribution of HRP among EVs in fraction F4. Association capacities of DSPE-PEG_{2000}-CH_3 / HRP mixture and unconjugated HRP controls remained constant without significant variation between 0.5µg/ml and 30µg/ml, with 40±21 HRP/EV and 28±6 HRP/EV respectively. Above this concentration, association capacities started to increase, reaching 341±289 HRP/EV and 134±39 HRP/EV at 75µg/ml, respectively. In contrast, DSPE-PEG_{2000}-HRP association to EVs started from 8±1 HRP/EV at 0.5µg/ml, and increased progressively to 21±10 HRP/EV at 1µg/ml, 154±56 at 10µg/ml and 272±76 at 30µg/ml to finally reach a plateau of 564±144 HRP/EV at 50µg/ml. Number of HRP associated with EVs was significantly higher than controls when HRP was conjugated with DSPE-PEG_{2000} for each tested concentration excepted at highest concentration (75µg/ml). This presence of

HRP with controls could be artifactual retention due to protein aggregation or limitation in SEC resolution as suggested by the observed high variability.

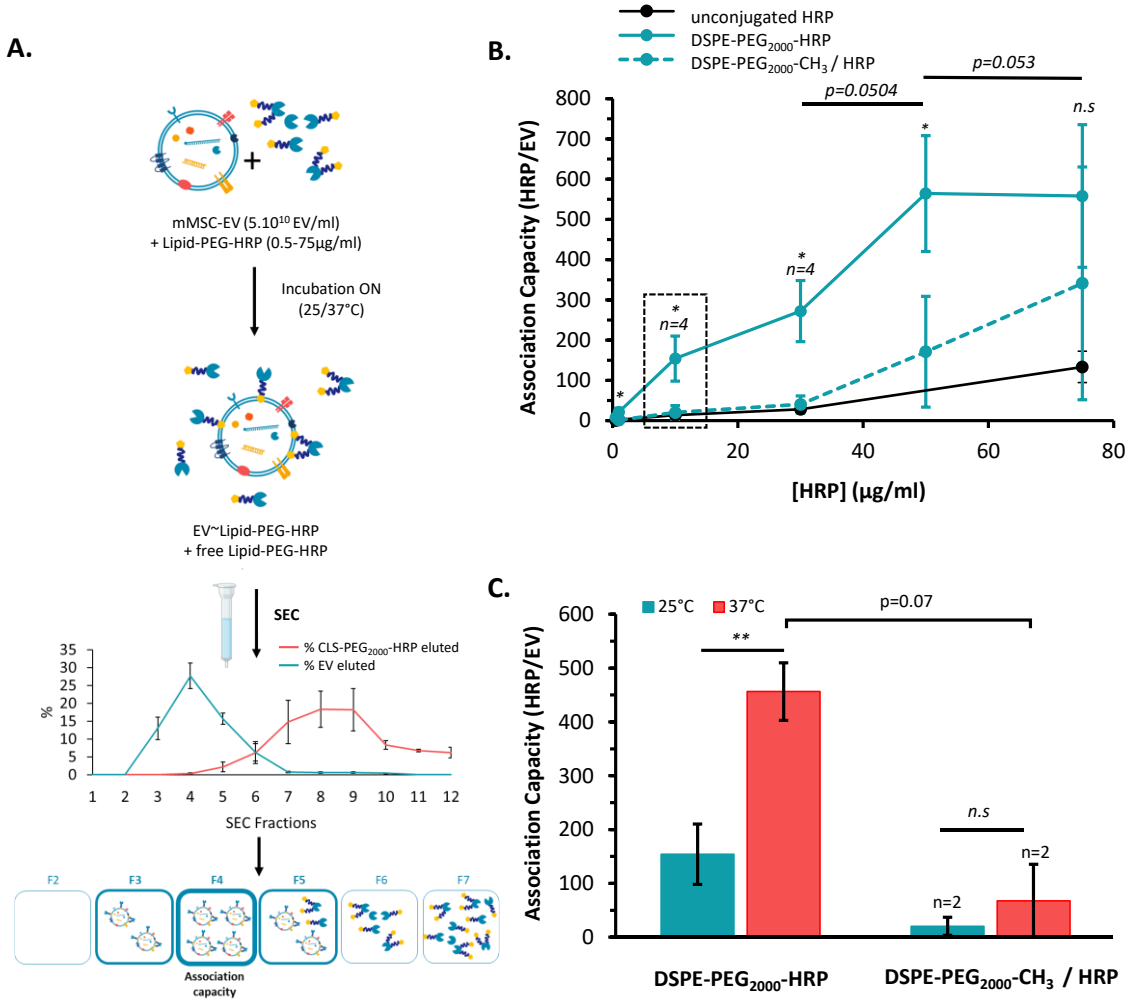

FIGURE 2 Influence of Lipid-PEG-HRP concentration and temperature on the association with EVs.
(A) Schematic representation of EV / Lipid-PEG-HRP association workflow (association, separation), not at scale. The 4th fraction of SEC was selected to calculate association capacity. **(B)** Number of biologically active Lipid-PEG-HRP per EV *vs.* HRP concentration after incubation of 5.10^{10} EV/ml with unconjugated HRP, unconjugated DSPE-PEG$_{2000}$-CH$_3$ / HRP, and DSPE-PEG$_{2000}$-HRP at 25°C overnight. n=3 if unspecified. Significance of p-values as compared to DSPE-PEG$_{2000}$-CH$_3$ / HRP control are given above each point as well as between two successive points. **(C)** Number of biologically active HRP conjugated per EV *vs.* temperature during incubation of 5.10^{10} EV/ml with 10µg/ml of DSPE-PEG$_{2000}$-CH$_3$ / HRP or conjugated DSPE-PEG$_{2000}$-HRP at 25°C or 37°C overnight. p-values were calculated using a two-tailed Welch test. *n.s*>0.05, *<0.05, **<0.01.

Regarding these results, an incubation concentration of 10µg/ml (framed in Figure 2B) was chosen for the following experiments in order to avoid EV surface saturation and favorize a good association efficiency (fraction of associated HRP as compared to initial incubated amount). Subsequently, the influence of incubation temperature (25°C or 37°C) was evaluated at this DSPE-PEG$_{2000}$-HRP concentration (Figure 2C). Interestingly, increasing the temperature of incubation from

25°C to 37°C enabled a rise in association from 154±56 HRP/EV to 456±53 HRP/EV while no significant increase was observed in the DSPE-PEG_{2000}-CH_3 / HRP control (20±17 HRP/EV at 25°C vs 68±68 HRP/EV at 37°C) despite an important variability. Noticeably, this value of 456±53 HRP/EV was close to EV saturation observed for higher DSPE-PEG_{2000}-HRP concentrations (50µg/ml) at 25°C. This incubation at 37°C was not deleterious for EVs based on mode, concentration and cryoTEM observations (Supplementary Figure 2). Therefore, association conditions were set to a Lipid-PEG-HRP concentration of 10µg/ml incubated at 37°C overnight with 5.10^{10} EV/ml for subsequent experiments.

2.1.2. Lipid-PEG anchor nature influences the HRP association to EVs

Three different MW of PEG linkers were compared for the same lipid anchor (DSPE) with 1000g/mol, 2000g/mol and 5000g/mol (Figure 3A), while cholesterol-PEG_{2000} (abbreviated in CLS-PEG_{2000}) was compared to DSPE-PEG_{2000} (Figure 3B). DSPE-PEG-HRP conjugates were efficiently associated to EVs without significant differences depending on the PEG MW, with an association capacity of 373±110 HRP/EV, 255±57 HRP/EV and 329±86 HRP/EV for DSPE-PEG_{1000}-HRP, DSPE-PEG_{2000}-HRP and DSPE-PEG_{5000}-HRP, respectively. By contrast, an association of 898±247 HRP/EV was obtained for CLS-PEG_{2000}-HRP as compared to 255±57 HRP/EV for DSPE-PEG_{2000}-HRP in the same conditions. Therefore, CLS-PEG_{2000} was selected as reference Lipid-PEG anchor for subsequent experiments and characterization.

In order to calculate association efficiency, i.e., the percentage of total available HRP that has been associated with EVs compared to the total amount introduced into the incubation media[33], all SEC fractions containing EVs (i.e., F3, F4 and F5) were considered (Figure 3C). First, controls without EVs were done to assess possible contamination of unconjugated HRP, DSPE-PEG_{2000}-HRP and CLS-PEG_{2000}-HRP in the pool. A low retention in considered SEC fractions of 3.8±3.1%, 2.6±2.1% and 2.3±1.8% were measured, respectively. After an incubation of 10µg/ml of unconjugated HRP, DSPE-PEG_{2000}-HRP or CLS-PEG_{2000}-HRP with EVs, association efficiencies of 3.1±2.9%, 9.7±3.3% and 33.2±0.5% were obtained, respectively.

2.1.3. CLS-PEG_{2000}-HRP association capacity depends on the EV donor cell source

As different methods of culture and isolation can lead to different EV sub-populations and contaminants and thus may induce different association capacities and cell internalization efficiencies, the versatility of this Lipid-PEG-based association method was evaluated for another source of mMSC-EVs. Therefore, in addition to commercial EVs used for previous experiments (mMSC-EV#1), EVs produced in our laboratory were also tested (mMSC-EV#2). Following the same association protocol, 701±213 HRP/EVs were obtained with mMCS-EV#2 in comparison to 1439±127 HRP/EV with mMSC-EV#1 (Figure 3D), highlighting an expected variation in association capacity depending on EVs

production and isolation protocol but also demonstrating the applicability of this approach to other EVs isolated with different methods.

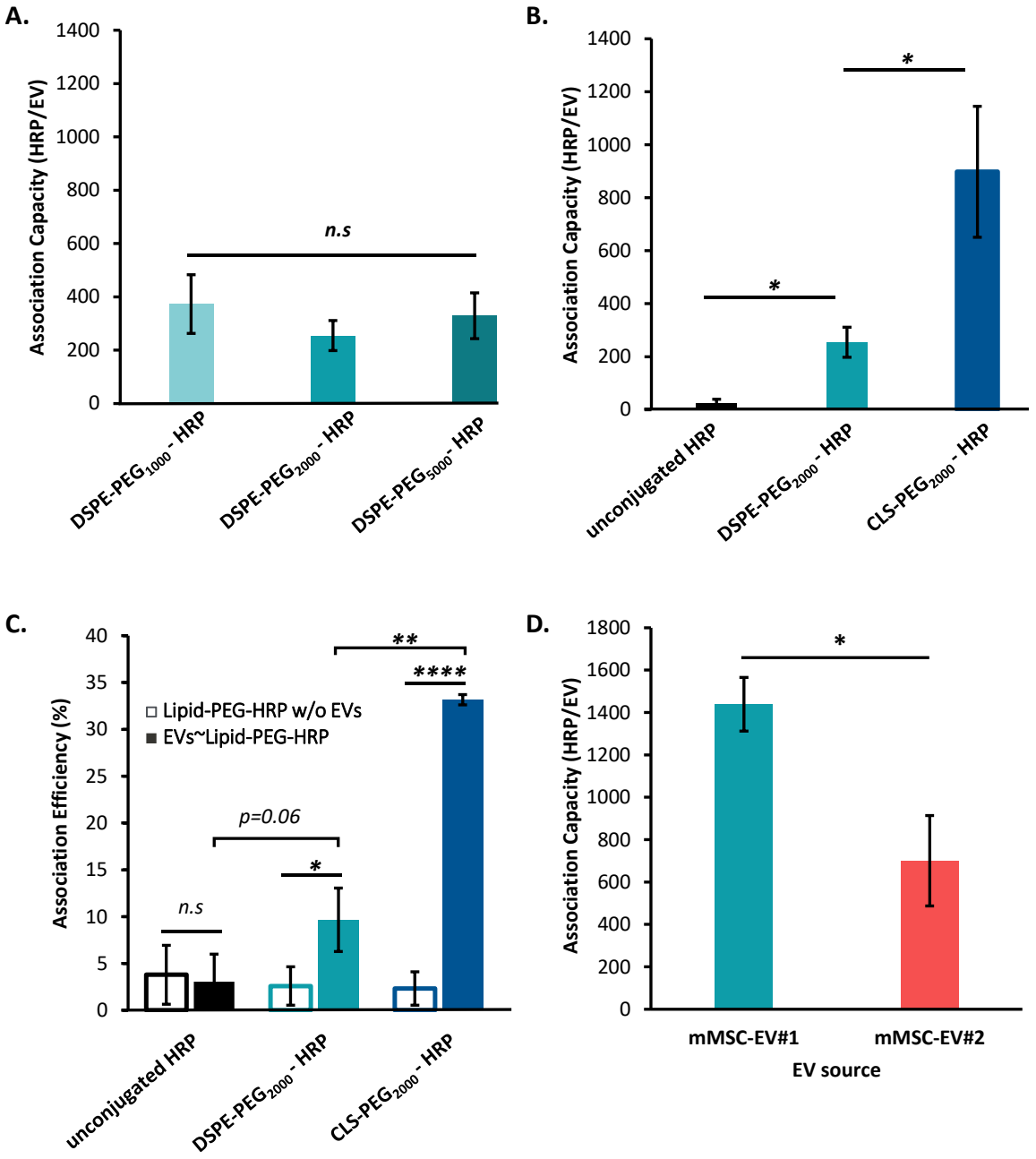

FIGURE 3 Influence of PEG linker MW, lipid anchor nature and EV type on the association between EVs and Lipid-PEG-HRP. Association efficiency according to **(A)** the PEG MW of DSPE-PEG anchor or **(B)** the lipid nature of Lipid-PEG$_{2000}$ anchor after incubation of 5.10^{10} EV/ml with 10µg/ml of HRP incubated overnight at 37°C. 4th SEC fraction was considered to calculate this association capacity. n=3. **(C)** Loading efficiency defined as percentage of Lipid-PEG-HRP retained with EVs after incubation of 10µg/ml of unconjugated HRP, conjugated DSPE-PEG$_{2000}$-HRP and conjugated CLS-PEG$_{2000}$-HRP with 5.10^{10} EV/ml (n=3) or without EVs (n=4) overnight at 37°C. **(D)** Association capacity of CLS-PEG$_{2000}$-HRP with mMSC-EV#1 or mMSC-EV#2. n=3. For **(C)** and **(D)**, all EV SEC fractions (F3, F4 and F5) were considered. p-values were calculated using a two-tailed Welch test. *n.s*>0.05, *<0.05, **<0.01, ***<0.001, ****<0.0001.

2.1.4. Single particle analysis of EV~CLS-PEG$_{2000}$-HRP-A488 association

In order to have an overview of the repartition of CLS-PEG$_{2000}$-HRP among EVs and to take into account bias resulting from the bulk-assumption of homogeneous distribution of the cargo, HRP was fluorescently labeled for single particle analysis measurements and co-localization observations. Unconjugated HRP and CLS-PEG$_{2000}$-HRP were conjugated with Alexa-Fluor 488 TFP ester to obtain unconjugated HRP-A488 and CLS-PEG$_{2000}$-HRP-A488. NTA analysis using Zetaview-Twin to measure particle concentration using two channels for light scattering and fluorescence (filter set at 500nm) showed no fluorescent particles for EVs incubated with unconjugated HRP-A488 while 59±14% of detected particles were fluorescent in EV~CLS-PEG$_{2000}$-HRP-A488 samples (Figure 4A).

NanoFCM analysis were carried out using Alexa647-coupled antibodies anti-CD9, -CD63 and -CD81 (Figure 4B). No A488+ particles were detected in control buffer containing CLS-PEG$_{2000}$-HRP-A488 alone (Supplementary Figure 3). Overall, 72%, 79% and 63% of fluorescent particles were A488+ in EV~CLS-PEG$_{2000}$-HRP-A488 after incubation with anti-CD9, -CD63 and -CD81 antibodies respectively. These values were 7%, 2% and 24% for EV / unconjugated HRP-A488. 27%, 24% and 20% of fluorescent particles were double positives for A488 and respectively CD9, CD63 and CD81 in EVs~CLS-PEG$_{2000}$-HRP-A488 sample in contrast to EV / unconjugated HRP-A488 showing respectively 1%, 1% and 6% of double positive EVs.

Super-resolution microscopy observations were done using DiI lypophilic dye and anti-CD9 antibody (Figures 4C&D). No unconjugated HRP-A488 or CLS-PEG$_{2000}$-HRP-A488 aggregates were detected as CD9/DiI/A488 triple positive clusters. 1±1% of mMSC-EV#1 / unconjug. HRP-A488 clusters were triple positive, in contrast with 14±1% and 42±2% for mMSC-EV#1~CLS-PEG$_{2000}$-HRP-A488 and mMSC-EV#2~CLS-PEG$_{2000}$-HRP-A488, respectively. Details in number of cluster-types are provided in Supplementary Figure 4.

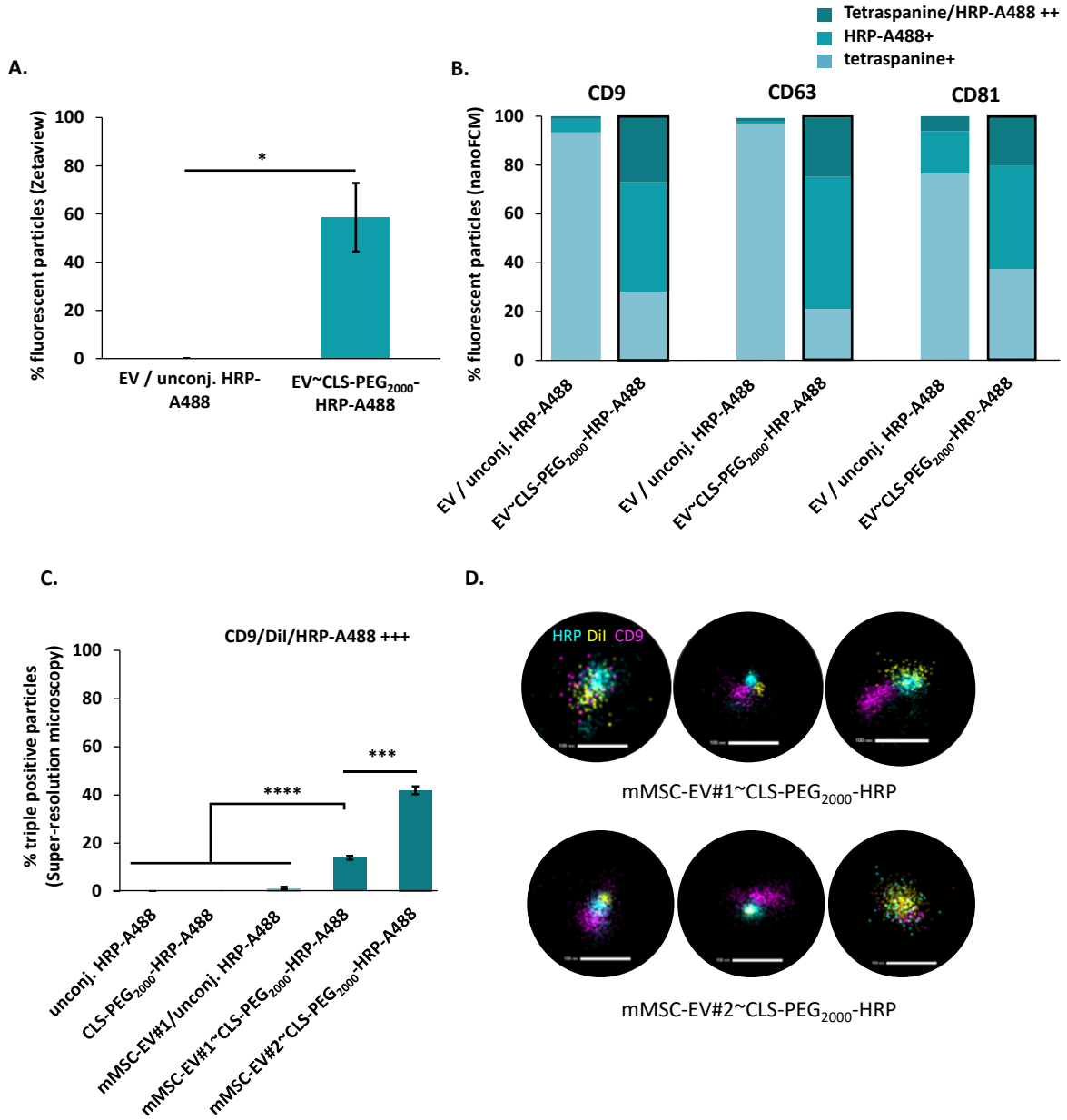

FIGURE 4 Fluorescence distribution of EV~CLS-PEG$_{2000}$-HRP-A488. (A) Proportion of fluorescent detected particles (mMSC-EV#1) using Zetaview (n=3) **(B)** NanoFCM analysis of mMSC-EV#1 after incubation with anti-CD9, anti-CD63 or anti-CD81 antibodies coupled with AlexaFluor647 (n=1). Only fluorescent particles have been considered. **(C)** Proportion of triple positive clusters using super-resolution microscopy. Samples were incubated with DiI dye and anti-CD9 antibody, while HRP was labeled with Alexa-Fluor 488 (n=3). **(D)** Representative images of triple positive clusters observed using super-resolution microscopy. p-values were calculated using a two-tailed Welch test. *n.s*>0.05, *<0.05, **<0.01, ***<0.001, ****<0.0001.

2.1.5. Lipid-PEG-HRP association does not modify EV size and surface characteristics

Because proteins are larger than usual cargos used with LA, conjugation impacts on physico-chemical properties of EVs were investigated. EV~CLS-PEG$_{2000}$-HRP (using mMSC-EV#1) were analyzed by NTA for size (Figure 5A) and Zeta Potential (ZP, Figure 5B). No significant changes neither in mode (110±4nm for EV~CLS-PEG$_{2000}$-HRP and 112±5nm for control) nor in negative ZP (-20±1mV for EV~CLS-PEG$_{2000}$-HRP and -19±1mV for control) were observed after association. EV / unconjugated HRP and EV~CLS-PEG$_{2000}$-HRP were compared by using MACSPlex Assay in order to evaluate the impact of the association on EVs antigens accessibility. Interestingly, EV~CLS-PEG$_{2000}$-HRP and control exhibited similar profiles (Figure 5C). 33 EV surface epitopes assessed by the test were detected in both types of EVs highlighting the preservation of the accessibility of EV surface antigens using this association method. No differences were visible using cryoTEM between EV samples associated or not with CLS-PEG$_{2000}$-HRP (Figure 5D).

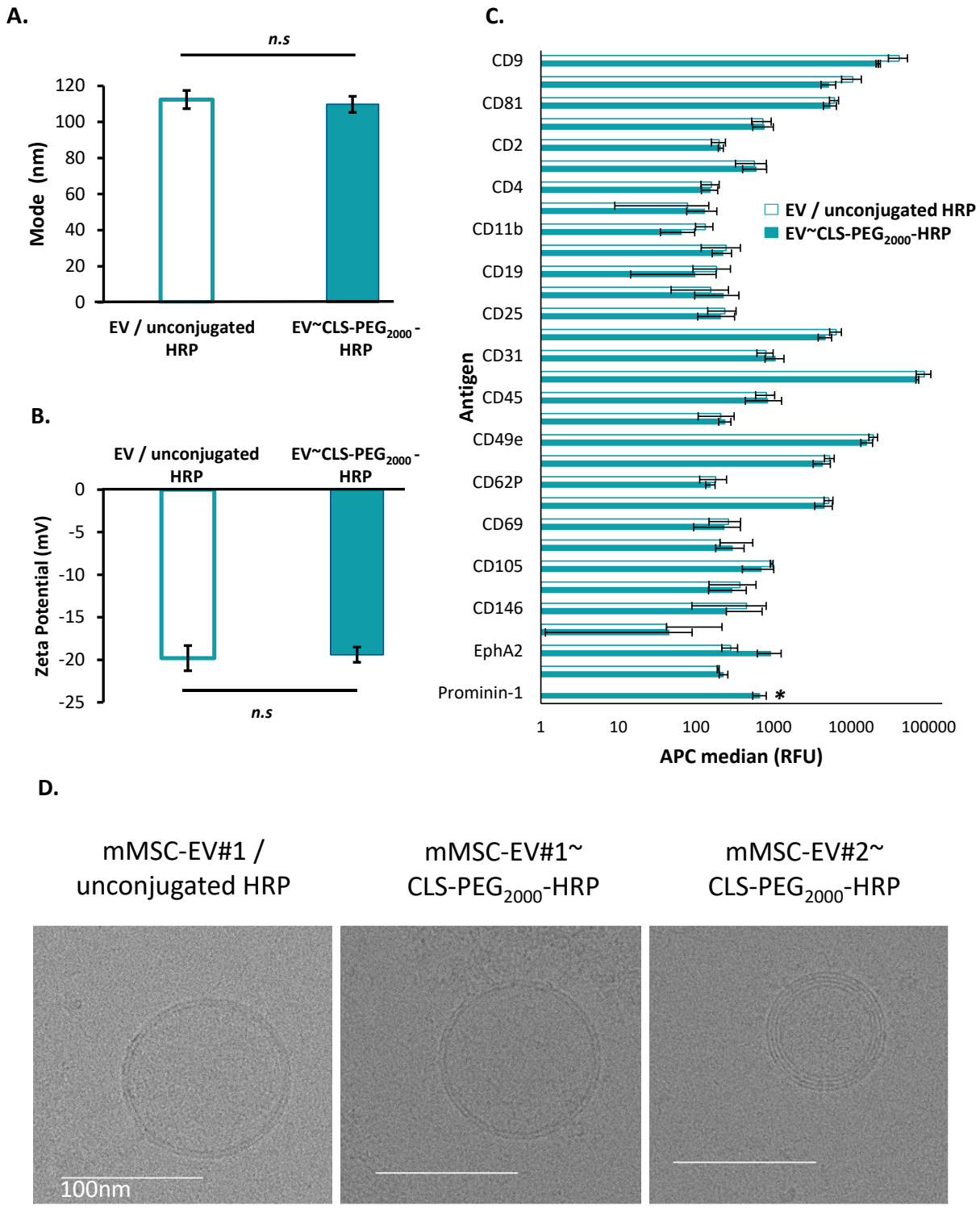

FIGURE 5 Characteristics of mMSC-EV associated or not with Lipid-PEG-HRP. (A) Size (mode, NTA, NS300, n=5) and (**B**) Zeta potential (NTA, Zetaview Twin, n=3) after incubation of mMSC-EV#1 with unconjugated HRP or CLS-PEG$_{2000}$-HRP and SEC separation. **(C)** MACSPlex Assay analysis as APC median after subtraction of buffer background signal. MHCI, CD326, CD115, CD41, CD40 and CD20 were removed from analysis due to high variability. p-values were calculated using a two-tailed Welch test and only Prominin-1 was significant (* p-value<0.05). **(D)** CryoTEM images of EVs after incubation with unconjugated HRP or CLS-PEG$_{2000}$-HRP. No SEC separation was processed on these samples. n=3.

2.1.6. Lipid-PEG-HRP anchorage to EVs demonstrates a good stability in presence of serum

A common reported issue using LA conjugation to EVs is the redistribution of the cargo to plasma components as reported in some studies with small LA-cargo[42,45]. For comparison purpose, similar stability study was carried out on EV~Lipid-PEG$_{2000}$-HRP with DSPE and CLS lipid. For the DSPE lipid (Figure 6A), 107±34%, 94±13%, 106±15% and 65±3% of the associated protein remained with EVs after 4°C ON in DPBS, a freeze/thaw (F/T) in DPBS, 37°C during 2 hours in DPBS or DPBS supplemented with Fetal Bovine Serum (FBS, 1:50), respectively. For CLS lipid (Figure 6B), these values were 75±16%, 159±52%, 83±14% and 71±1%, respectively. Overall, these results showed a good stability of the anchorage with EVs despite some partial redistribution of Lipid-PEG-HRP to FBS components.

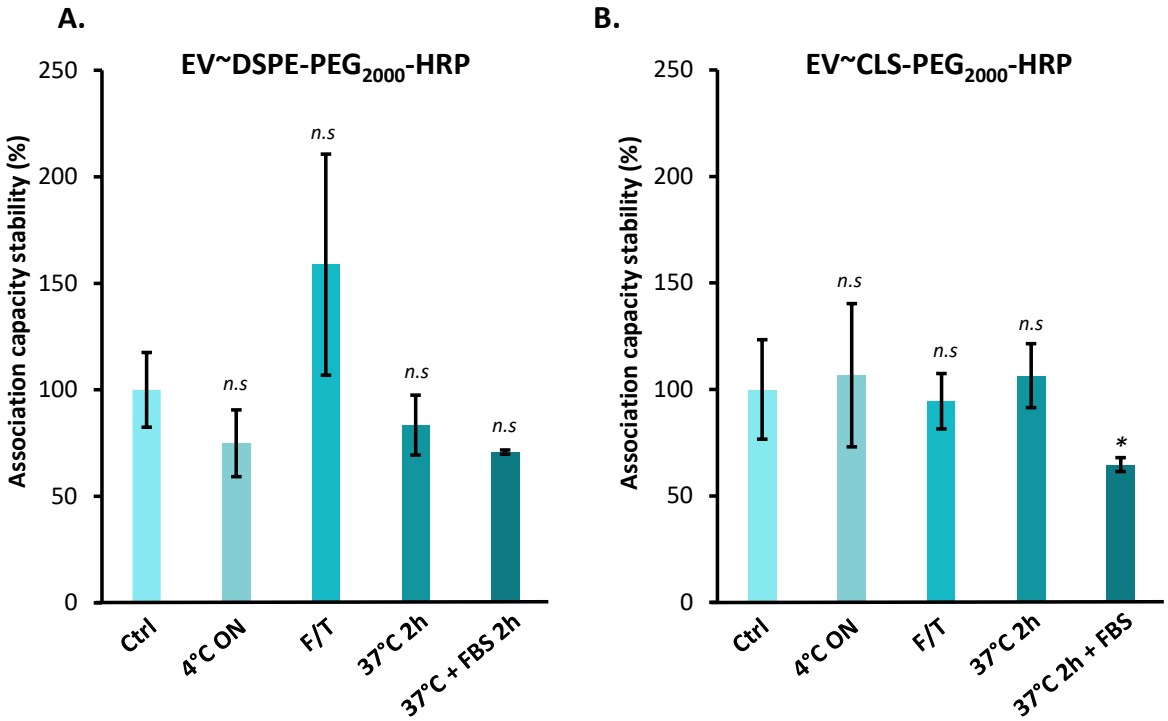

FIGURE 6 Stability of the EV / Lipid-PEG$_{2000}$-HRP association. Association capacity of DSPE-PEG$_{2000}$-HRP **(A)** and CLS-PEG$_{2000}$-HRP **(B)** in percentage of control samples. Samples were diluted at 1:11 in DPBS (or DPBS supplemented with 1:50 FBS if indicated) and incubated before SEC separation. **4°C ON** samples were incubated at 4°C ON, **F/T** were frozen at -80°C before thawing, and **37°C 2H (+FBS)** were incubated at 37°C during 2h either with DPBS or DPBS + 1:50 FBS. n=3 except for CLS-PEG$_{2000}$-HRP 4°C ON (n=2). p-values were calculated using a two-tailed Welch test and samples were compared with Ctrl. n.s>0.05, *<0.05.

2.2. Absolute quantification of cellular uptake of functional HRP using Lipid-PEG anchorage to EVs

2.2.1. EV association enables concentration- and time-dependent intracellular delivery of active Lipid-PEG-HRP into PANC-1, A549 and SKBR3 cells

In order to study the ability of EVs to deliver intracellularly a functional anchored enzyme and to provide an absolute quantification of this internalization, EV~Lipid-PEG-HRP samples were incubated with 1.10^5 PANC-1 cells (adherent epithelioid carcinoma cell line derived from human pancreas) per well. Cells were subsequently washed before lysis and HRP enzymatic activity was measured in cell lysate. M-PER™ lysis buffer was observed to increase in a linear and reproducible way the enzymatic activity of HRP as compared to DPBS (data not shown) probably by crowding effect due to surfactants[46]. Therefore, all sample dilutions and standard curves were done in lysis buffer for enzymatic assay. This enabled us to precisely measure the mass of internalized HRP per 1.10^5 cells. Moreover, control conditions with identical amount of Lipid-PEG-HRP without EVs were performed as the hydrophobic properties of Lipid-PEG-HRP could potentially favor its internalization without EVs as vectors, either by direct interaction with cells or mediated by adsorption with FBS components. For all cellular experiments, the amount of HRP incubated with cells was fixed (except when specified). As a consequence, the number of EVs per cell was variable between experiments depending on the EV/HRP association capacity but remained in the range of 500-2000 EVs/cell. Importantly, all these experiments were done in presence of FBS in order to verify the stability of the anchorage suggested by the previous stability experiment.

First, EV~CLS-PEG$_{2000}$-HRP were tested for cell internalization at different HRP amounts (1ng, 5ng, 10ng and 15ng per well, Figure 7A). While native EVs without HRP did not trigger any peroxidase activity in PANC-1 cells lysate, validating the absence of detectable endogenous peroxidase activity, a slight increase in HRP activity was observed when cells were treated with free CLS-PEG$_{2000}$-HRP control from 3±1pg recovered at 1ng incubated to 64±9pg recovered at 15ng incubated. By contrast, a significant increase in HRP activity recovered in cell lysate was observed when cells were incubated with EV~CLS-PEG$_{2000}$-HRP: from 18±2pg at 1ng/well to 310±50pg at 15ng/well incubated (Figure 7A). Interestingly, the HRP activity recovered in cell lysate was strongly proportional to the amount of EV-associated enzyme incubated with cells (R^2=0.999) and no plateau was reached in these conditions. Incubation time impact on HRP internalization was assessed after 2h, 4h and 24h for an amount of HRP fixed at 10ng/well (Figure 7B). Internalized HRP increased over time from 14±2pg after 2h to 27±4pg after 24h for CLS-PEG$_{2000}$-HRP control and from 56±5pg after 2h to 194±27pg after 24h for EV~CLS-PEG$_{2000}$-HRP. Impact of the temperature on cell internalization was also studied (Figure 7C). Only 4±1pg and 15±4pg of HRP were recovered at 4°C compared to 8±2pg and 97±12pg at 37°C for CLS-PEG$_{2000}$-

HRP control and EV~CLS-PEG$_{2000}$-HRP respectively, suggesting a temperature-dependent internalization process.

Impact of EV-producing cell line was also studied by comparing internalization of mMSC-EV#1~CLS-PEG$_{2000}$-HRP and mMSC-EV#2~CLS-PEG$_{2000}$-HRP in PANC-1 cells (Figure 7D). Because these two samples were associated with different amount of HRP, different number of EVs were deposited with cells to incubate them with same HRP mass (10ng incubated, thus 891 to 1087 mMSC-EV#1 per cell *vs*. 1557 to 1894 mMSC-EV#2 per cell). 215±13pg and 143±12pg of HRP were recovered in PANC-1 lysate after incubation with mMSC-EV#1 and mMSC-EV#2, respectively.

Finally, two other recipient cells lines were tested in addition to PANC-1 cells, namely A549 and SKBR3 cells which are adherent epithelioid carcinoma cell line derived from human lung and breast respectively (Figure 7E), in order to evaluate the versatility in protein delivery of this approach for other cell lines. Whatever the cell line, 1.10^5 cells were harvested and similar confluency of 80% was obtained for each cell line after 24h prior to incubation with mMSC-EV#1~CLS-PEG$_{2000}$-HRP. 358±16pg, 230±21pg and 119±55pg of HRP were recovered in cells lysates of A549, PANC-1 and SKBR3 cells respectively after 4h of incubation with 10ng of HRP, demonstrating the ability of EV~CLS-PEG$_{2000}$-HRP to be internalized in different human adherent epithelioid carcinoma cell line *in vitro*.

A549 cell internalization was observed using epifluorescence microscopy (Figure 8A to 8E). For these experiments, unconjugated HRP-A488 and CLS-PEG$_{2000}$-HRP-A488 were separated from EVs using ultrafiltration instead of SEC in order to limit their dilution and to obtain enough fluorescent signal. Controls were done with identical HRP and EV concentrations to make sure that no contamination was responsible for internalized fluorescence. Fluorescent spots were only visible in EV~CLS-PEG$_{2000}$-HRP-A488 (Figure 8E). Quantitative analysis was applied using confocal microscopy on these samples. 3D image stacks were analyzed using a random-forest algorithm to determine the number of fluorescent spots inside cells (Figure 8F). 52±6 spots per 1.10^6 voxels were detected in EV~CLS-PEG$_{2000}$-HRP-A488 in contrast to controls that presented <1 spot per 1.10^6 voxels. Taken together, these results confirmed quantitative cell lysis experiments.

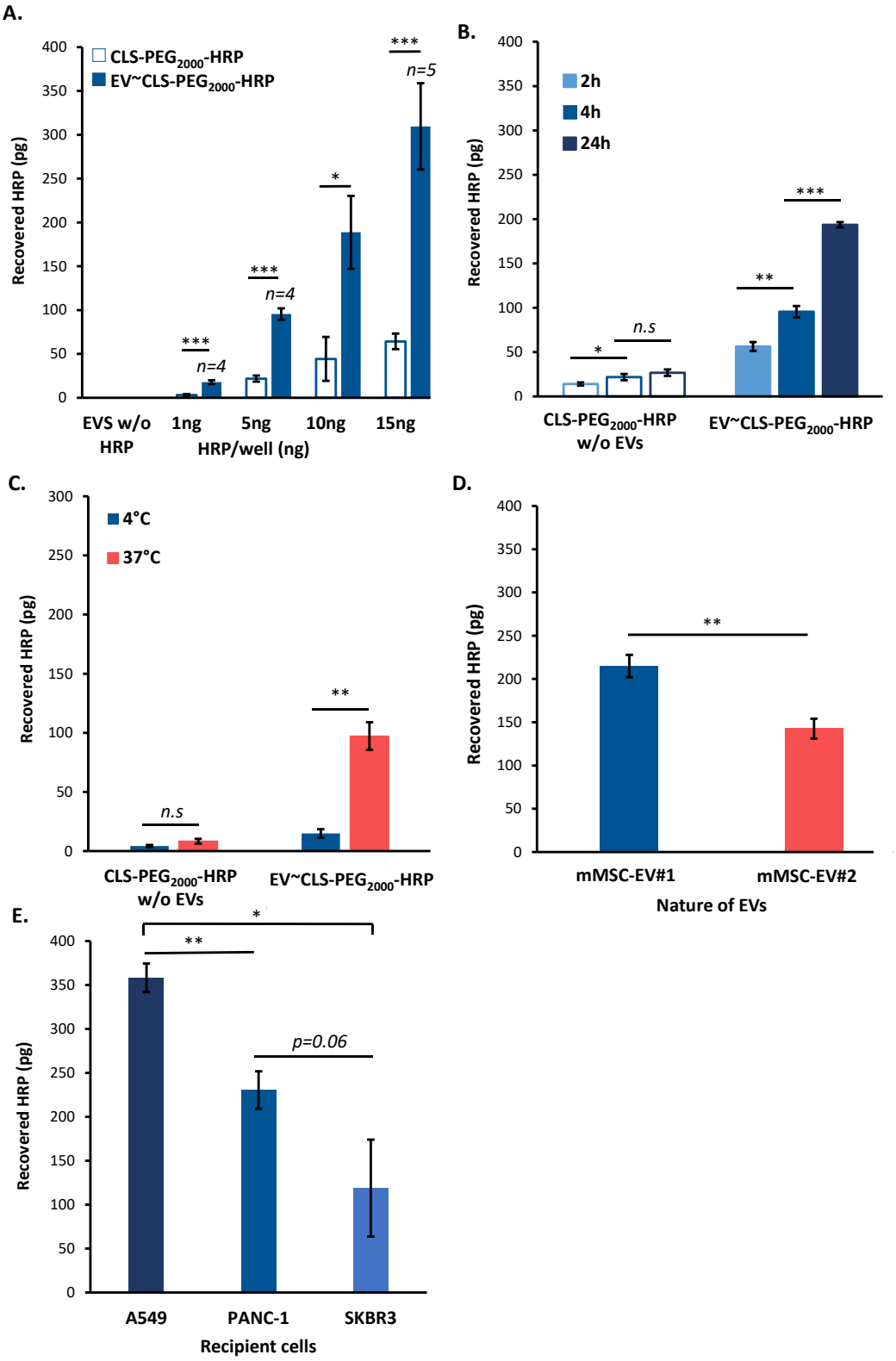

FIGURE 7 Quantification of absolute amount of internalized HRP depending on quantity, temperature and incubation time on cell internalization of EV~CLS-PEG$_{2000}$-HRP. Recovered CLS-PEG$_{2000}$-HRP vectorized or not by EVs in PANC-1 lysate after incubation with 1.10^5 PANC-1 following these conditions: **(A)** 4h, 37°C, **1ng, 5ng, 10ng or 15ng** of HRP/well. **(B) 2h, 4h or 24h** of incubation, 37°C, 5ng/well of HRP. **(C)** 2h, **4°C or 37°C**, 10ng/well of HRP. **(D)** Incubation 4h, 37°C, 10ng/well of EV~CLS-PEG$_{2000}$-HRP vectorized by **mMSC-EV#1 or mMSC-EV#2**. **(E)** 4h, 37°C, 10ng with 1.10^5 **A549, PANC-1 or SKBR3 cells**. For each experiment, p-values were calculated using a two-tailed Welch test. *n.s*>0.05, *<0.05, **<0.01, ***<0.001. n=3 if unspecified.

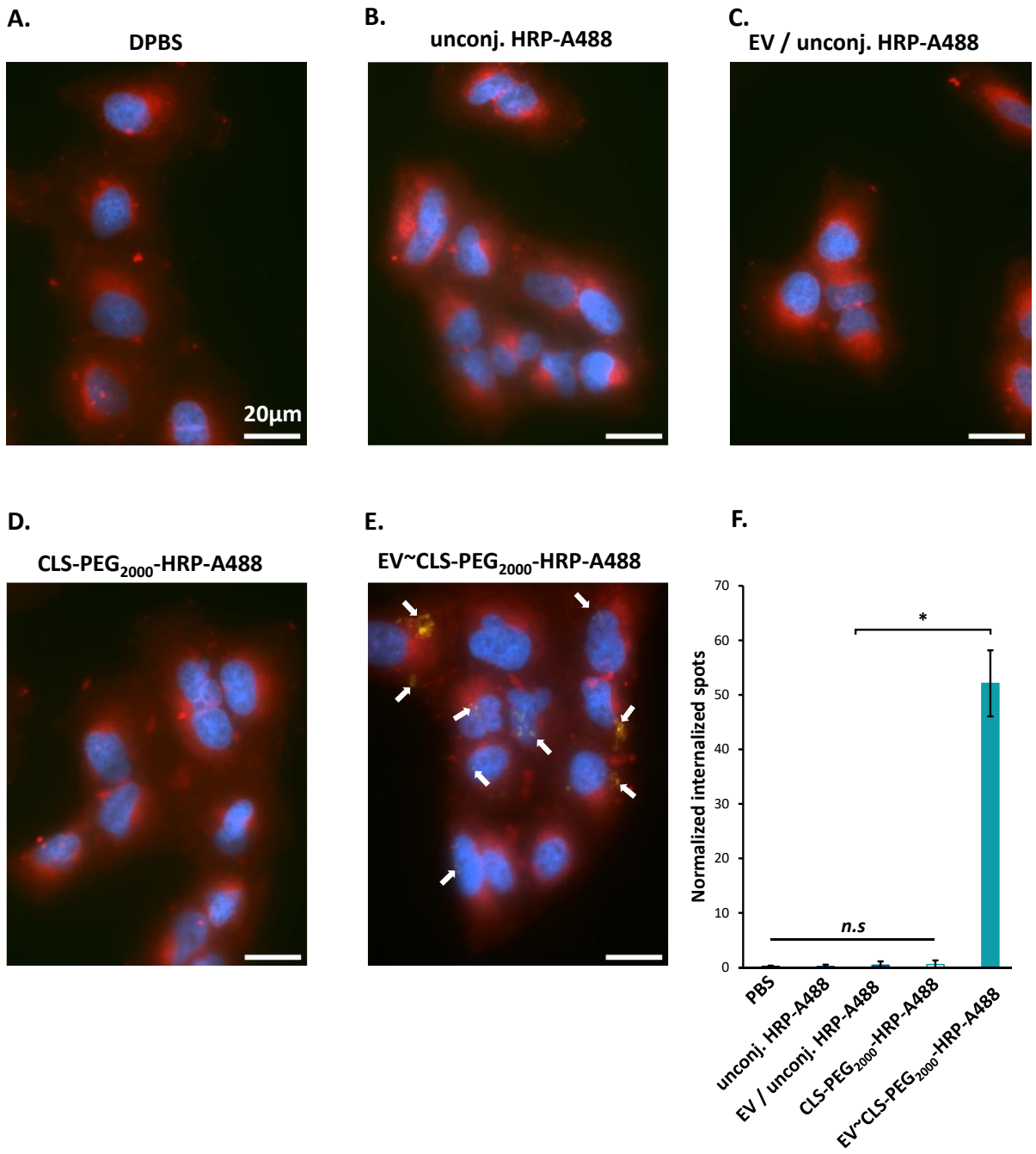

FIGURE 8 Epifluorescence microscopy observation and confocal quantification of HRP-A488 cell internalization. A549 cells were incubated 4 hours with HRP-A488, conjugated with CLS-PEG$_{2000}$ or not and associated with EVs or not. Panel images have been acquired using full-field epifluorescence microscopy. Blue, Red and green fluorescence are DAPI, Cell Mask lipophilic dye and Alexa-fluor 488 from labeled HRP, respectively. **(A)** A549 cells control incubated with DPBS. **(B)** and **(C)** A549 cells incubated with unconjugated HRP-A488 alone and mixed with EVs, respectively. **(D)** and **(E)** A549 cells incubated with CLS-PEG$_{2000}$-HRP-A488 alone and associated with EVs, respectively. Identical HRP mass was deposited between EV conditions and their respective controls. Identical number of EVs was deposited between EV conditions. Bar scale is 20µm. White arrows highlight some HRP-A488 spots. **(F)** Quantitative analysis on confocal 3D image stacks obtained using spinning-disk confocal microscopy. Number of fluorescent spots in cells was normalized per total number of voxels corresponding to intracellular space. n=2 images except for EV / unconj. HRP-A488 (n=3). For each experiment, p-values were calculated using a two-tailed Welch test. *n.s*>0.05, *<0.05.

2.2.2. Lipid-PEG linker MW impacts cell internalization of EVs~Lipid-PEG-HRP

Finally, impacts of lipid and PEG moieties of Lipid-PEG anchors on the cell internalization were evaluated (Figure 9A). Lipid-PEG-HRP alone controls were internalized at 29±7pg, 3±2pg, 1.2±0.3pg and 3±1pg for CLS-PEG$_{2000}$-HRP, DSPE-PEG$_{1000}$-HRP, DSPE-PEG$_{2000}$-HRP and EV~DSPE-PEG$_{5000}$-HRP respectively. While unconjugated HRP showed no cell internalization, EV~CLS-PEG$_{2000}$-HRP, EV~DSPE-PEG$_{1000}$-HRP, EV~DSPE-PEG$_{2000}$-HRP and EV~DSPE-PEG$_{5000}$-HRP were internalized at 124±22pg, 140±8pg, 87±4pg and 12±5pg respectively. Regarding these results, it seemed that the PEG linker MW influenced strongly the cell internalization efficiency, and it was hypothesized that this could be due to steric hindrance.

To assess this assumption, the influence of a decreased number of Lipid-PEG-HRP associated per EV on relative cell internalization was investigated (Figure 9). Indeed, the amount of HRP per EV can be fine-tuned depending on Lipid-PEG-HRP concentration added during incubation with EVs (Figure 2B). Interestingly, no change in cell internalization was observed whatever the HRP/EV ratio for EV~CLS-PEG$_{2000}$-HRP (from 1503 to 33 HRP/EV, Figure 9B) and EV~DSPE-PEG$_{1000}$-HRP (from 447 HRP/EV to 85 HRP/EV, Figure 9C). However, a decrease from 337 HRP/EV to 171 HRP/EV and 84 HRP/EV for EV~DSPE-PEG$_{5000}$-HRP resulted in an increase of 1.4±0.1 and 2.1±0.3 fold-change in cell internalization, respectively (Figure 9D). These results tend to indicate that steric hindrance of DSPE-PEG$_{5000}$-HRP may indeed be implied in its lower internalization as compared to other tested EV~Lipid-PEG-HRP and underline the interest of wisely control EV surface engineering to maintain the EV ability to interact with target cells.

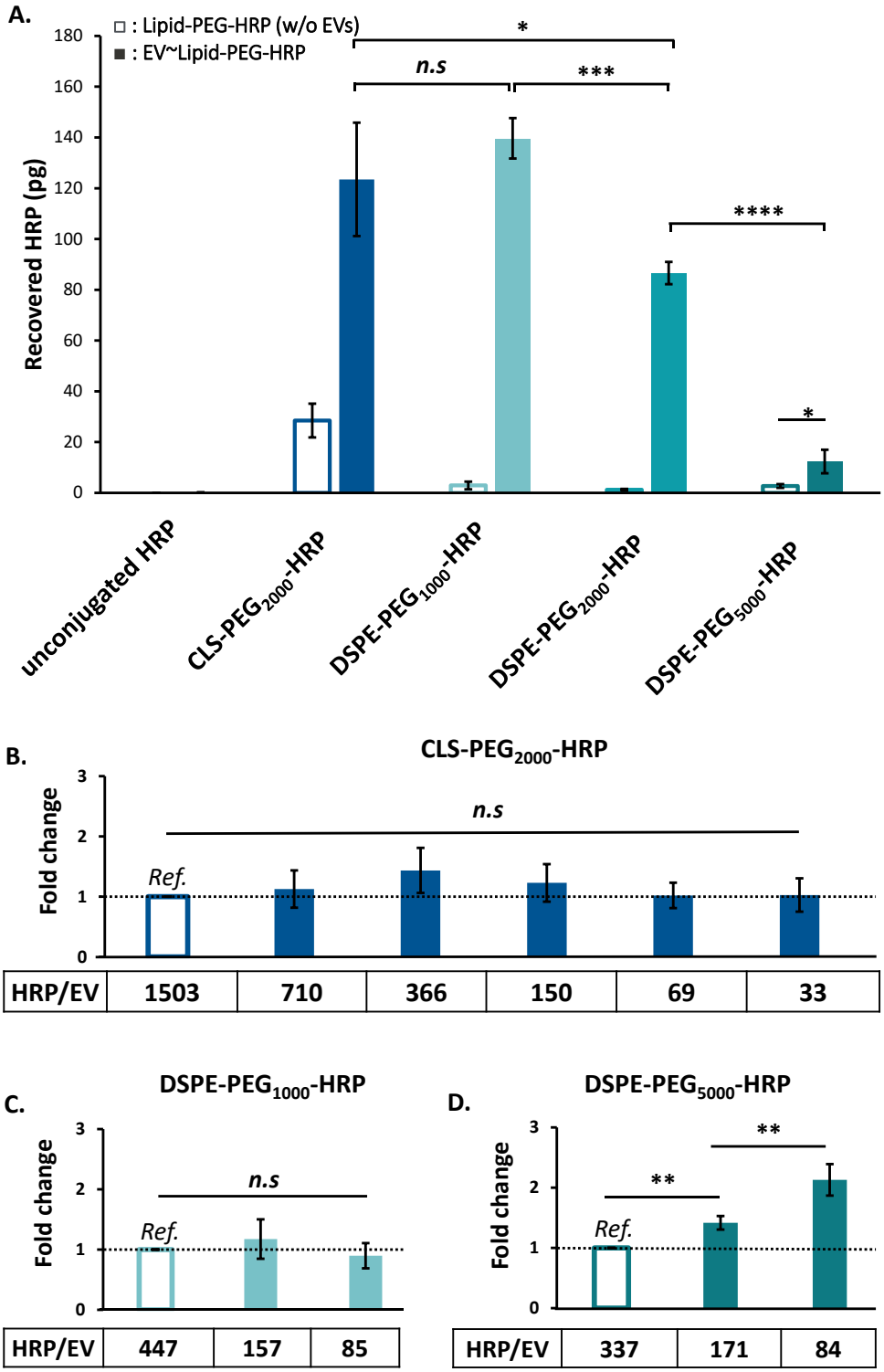

FIGURE 9 Impact of lipid anchor nature, PEG linker MW and HRP/EV ratio on cell internalization. (A) Recovered Lipid-PEG-HRP in PANC-1 lysate after incubation of 10µg of Lipid-PEG-HRP associated or not to EVs, for 4h at 37°C with 1.10^5 PANC-1 cells. n=4. **(B), (C) and (D).** Fold change in recovered Lipid-PEG-HRP in PANC-1 lysate after incubation of 1500 EV~Lipid-PEG-HRP per cell for 4h at 37°C with 1.10^5 PANC-1 cells. Decreasing HRP/EV ratio have been tested with CLS-PEG$_{2000}$-HRP, DSPE-PEG$_{1000}$-HRP and DSPE-PEG$_{5000}$-HRP for **(B)**, **(C)** and **(D)**, respectively. Proportion of Lipid-PEG-HRP recovered in lysate was normalized with the highest ratio of the experiment (indicated on figure as *Ref.*). Significances are compared to 1 (null hypothesis = no changes whatever the HRP/EV ratio). n=3. For each experiment, p-values were calculated using a two-tailed Welch test. *n.s*>0.05, *<0.05, **<0.01, ***<0.001, ****<0.0001.

3. Discussion

Lipid-anchorage is a versatile approach compatible with protein cargos while maintaining their activity

The main aim of this study was to provide a versatile and convenient way to associate exogenous cargo proteins to EVs for cellular uptake and to provide accurate absolute metrics. Indeed, to the best of our knowledge, no cellular internalization of an active protein associated with EVs using this LA-based approach has been reported for now. Moreover, only a very limited number of studies investigated this approach for protein association to EVs, and only for surface displaying purpose (e.g., cancer cells targeting[43] and EV-based vaccine[23]). Because a protein is more prone to loss its activity after internalization than its antigenicity as studied in Wang *et al*.[23], we wanted to investigate LA-conjugation for cellular uptake of an active protein. Unfortunately, few studies have reported the absolute amount of cargo internalized by cells, which makes interstudy comparisons difficult. Metrics are often relative (e.g., expressed in fold-increase as compared to control condition or in percentage of positive cells) and mass of internalized cargo is rarely directly measurable. Finally, these measurements are often based on fluorophores that can generate artifacts (e.g., dye or denatured cargo aggregates that are not discriminated from EVs) or antibodies detection which can be limited by steric hindrance if high amount of cargo is associated with EVs[47].

Hence, we chose here to use the HRP for its sensitive enzymatic activity to study the interest of a strategy relying on lipid anchor. This functional readout enabled us to assess only active proteins in order to exclude potential HRP aggregates or denaturated HRP from our association calculation. SEC was chosen to separate EVs and free HRP, since our controls showed no significant contamination of EVs by free Lipid-PEG-HRP after separation. Finally, we chose to use a click-chemistry reaction between maleimide and thiol to associate Lipid-PEG and HRP. This reaction is easy to use, efficient, quick, compatible with biomolecules in water and specific, enabling the conjugation of LA to virtually all proteins. Cysteines can be directly targeted by maleimides to provide relatively specific reaction sites due the limited number of accessible reduced cysteines in natural proteins, or maleimides can be introduced by using sulfo-SMCC to target lysines if proteins do not exhibit cysteines (as HRP in this study). Thus, one of the strengths of this approach is the possibility to adapt the conjugation strategy to the cargo protein to be delivered.

LA conjugation enables efficient association of HRP to EVs while preserving their properties

We determined that while no unconjugated HRP was loaded by simple incubation, up to 898±247 CLS-PEG_{2000}-HRP were associated per EV (Figure 3B). This magnitude of order in associated proteins per EV is consistent with the recent study of Wang *et al*. using ELISA assay[23]. By optimizing the amount of cargo protein during incubation, an association efficiency of 33.2±0.5% was reached in these

conditions (Figure 3C), which is among best protein loading efficiencies with EV reported into the literature[33]. Moreover, only 63±15% of EVs were recovered after SEC, probably leading to an underestimation of the total fraction of HRP associated with EVs due to the loss of EV~Lipid-PEG-HRP. Assuming that SEC did not discriminate EV~Lipid-PEG-HRP and unassociated EVs, it could be proposed from the 898 CLS-PEG_{2000}-HRP/EV ratio that 53% of CLS-PEG_{2000}-HRP was actually associated to EVs before SEC separation. Importantly, association calculations were done based on the "bulk-approach", assuming an homogeneous distribution of HRP among EVs because all EVs are enclosed by a bilayer membrane, but should be carefully considered in regard to recent studies reporting EV encapsulation heterogeneity[48]. We used three different analysis methods to characterize this heterogeneity, namely fluorescent NTA, nano-flow cytometry and super-resolution microscopy. Overall, up to 70% of particles were HRP-A488+ (Figures 4A&B), among which half were tetraspanins+ (Figure 4B) according to nano-flow cytometry measurements. Interestingly, three-fold more CD9/DiI/HRP-A488 triple positive particles were detected in mMSC-EV#2 using super-resolution microscopy (Figure 4C), which could indicate the presence of HRP-associated contaminants in mMSC-EV#1. Contamination could also explain higher fraction of retained CLS-PEG_{2000}-HRP with mMSC-EV#1 as compared to mMSC-EV#2 (Figure 3D). This supports observations already done by other groups[45,48] suggesting that the presence of contaminants can be a major problem affecting loading efficiency. However, it is to note that a negative particle for a given tetraspanin could also be an EV. This heterogeneity in association distribution suggests that LA-protein preferentially anchors in some subtypes of particles that remain to be determined.

The choice of LA is crucial for protein association to EV surface

We showed that cholesterol (CLS) was 3.5-fold more efficient for EV association than DSPE with mMSC derived EVs (Figure 3B). This greater affinity of CLS could be due to the cholesterol condensing effect[49] combined to its natural presence in high amount in EV membrane[50]. Supporting this assumption, a recent study[45] demonstrated the ability of EV membrane to insert up to 20% exogenous cholesterol in addition to endogenous cholesterol, instead of replacing it. Interestingly, this outperformance by the cholesterol anchor has also been observed for siRNA/EV association[37,51] but not by some other teams working with smaller chemical-LA. Indeed, a lack of efficiency from fluorescent NBD conjugated cholesterol (CLS-NBD) to label EVs has been observed in addition to the formation of CLS-NBD aggregates[42]. By contrast, in our study, efficient anchorage and a lack of CLS-PEG_{2000}-HRP aggregates were observed. These differences could be explained by the lower concentration of CLS-PEG_{2000}-HRP incubated with EVs in our study (3.10^3 molecules per EV in regard to 3.10^4 for Zheng *et al*[42]). The presence of the hydrophilic PEG linker as well as the nature of the cargo conjugated to cholesterol may sterically prevent aggregation to some extent. EV-producing cell origin

and EV isolation methods could also play a role by affecting EV membrane composition, corona and contaminants that could be in competition with EVs for association with HRP. It is to note that some other studies have described alternative lipids than cholesterols for association with EVs, such as DOPE[42] or a-tocopheryl succinate[51] that remain to be tested.

Nevertheless, if the lipid anchorage approach has many advantages, the main limitation is that the cargo will very likely be exposed on the EV surface. For this reason, the term "association" was used in this study rather than "loading". Exposing the protein of interest could be an issue if the cargo is accessible to proteases. However, it is also known that attachment of proteins can increase their resistance to proteases by decreasing the accessibility of their cleavage sites, as described in the literature for HRP[52]. It is also possible that EV corona protects anchored proteins along with adsorbed serum protein.

Lipid Anchorage of a protein to EVs enables its intracellular delivery depending on LA properties

After successful association study and optimization, intracellular delivery of HRP was investigated. Regarding these results, CLS-PEG_{2000} and a ≈1000 HRP/EV ratio were chosen as standard conditions. Although the association of HRP could probably be further increased, it did not seem appropriate to run the risk of impeding EV receptor's accessibility, that might be crucial for cell internalization. The high number of HRP associated per EVs obtained in this study enabled the use of relatively low amount of EVs to treat cells, with 200 to 2000 EVs per cell depending on the desired amount of incubated HRP, a dose compatible with cargo-specific cell response as recently established[53].

Using this approach, it was possible to determine the absolute amount of HRP uptake by cells. Under these physiological conditions and the presence of serum, no unconjugated HRP was internalized, while a small amount of CLS-PEG_{2000}-HRP was internalized without EVs, probably due to the affinity of cholesterol for biological membranes. Interestingly, this low internalization of free control Lipid-PEG-HRP in plasma suggests that redistributed HRP to plasma components is likely not internalized by cells, ruling out the risk of artifactual internalization due to EV~Lipid-PEG-HRP destabilization. By contrast, association and vectorization of CLS-PEG_{2000}-HRP with EVs enabled up to 10 folds more intracellular delivery in three different carcinoma-derived cell lines (PANC-1, A549 and SKBR3 cells). Taken together, these results suggest that proteins could be more stable cargos for lipid anchorage than small chemicals in presence of serum. Some differences in HRP delivery were observed among cell types, confirming the already described phenomenon that EV internalization can differ depending on cell type[22]. Interestingly, this delivery was concentration-, time- and temperature-dependent, allowing for a fine tuning of the amount that can be delivered. Unfortunately, it is difficult

to compare these masses of internalized HRP with literature since such absolute measurements are barely ever reported.

Finally, the impact of three PEG linker MW on cell internalization was investigated for the same lipid (DSPE). Interestingly, while the PEG MW did not appear to be a significant parameter influencing protein association to EVs, it seemed to heavily influence cell internalization. Indeed, when the HRP was associated to EVs with a high MW PEG linker (5000g/mol), the cell internalization efficiency was significantly decreased. This effect was mitigated by decreasing the number and therefore density of DSPE-PEG_{5000}-HRP per EV. It can be hypothesized that steric hindrance from large cargo as well as hydrophilic properties of PEG hinder EV/cell membrane interactions (despite being unexpected at low covering density[54]). Such impact of the LA linker on EV / LA-cargo association and cellular uptake is rarely studied and should probably be further investigated.

4. Conclusion

While EVs are promising biomolecule vectors, their membrane is as impermeable to proteins as the cellular one. Thus, reaching acceptable protein loading/association capacity and intracellular uptake remains an important challenge, using either endogenous or exogenous approaches. Here, Lipid-Anchor conjugation of an enzyme using cholesterol-PEG or DSPE-PEG was shown to enable efficient association with mMSC-derived EVs followed by cellular uptake even in the presence of serum. Using enzymatic activity of HRP to provide absolute metrics, it was possible to control the number of HRP associated to EV surface, allowing for efficient and tunable intracellular delivery. We hope that these data will enable comparison with future studies using this approach and other methods. These results prove the particular interest to thoroughly characterize EV-association processes with the aim to preserve their natural properties for cell interaction. In order to improve this process, other molecules such as lipids and polymers could be investigated. In particular, the effect of the PEG linker has been by far less studied than lipid impact whatever the cargo, despite being crucial as showed in this study. Altogether, these results demonstrate that exogenous association of active proteins to EVs using LA is possible and can lead to the formation of an efficient intracellular delivery system. This clearly opens exciting perspectives for different protein replacement or inhibition therapies.

5. Materials and methods

5.1. Chemicals

Chemicals were purchased from (i) Biopharma PEG (USA): DSPE-PEG$_{1000}$-SH, DSPE-PEG$_{2000}$-SH, DSPE-PEG$_{5000}$-SH, CLS-PEG$_{2000}$-SH (structures are shown in Supplementary Figure 1A); (ii) Sigma-Aldrich (France): sepharose CL-2B cross-linked, sulfuric acid 95-97%; formic acid 98-100%; acetonitrile 99%, trehalose, Tris-HCl; (iii) Thermofisher (France): EZ-Link™ Maleimide Activated Horseradish Peroxidase, ELISA 1-Step™ Ultra TMB, M-PER™ Mammalian Protein Extraction Reagent, Pierce™ Protease Inhibitor Mini Tablets, CellMask™ Plasma Membrane Stains, DAPI, ProLong™ Gold Antifade Mountant; (iv) Gibco LifeTechologies (USA): Dulbecco's Modified Eagle Medium (DMEM), Foetal Bovine Serum (FBS), penicillin/streptomycin, L-glutamine, trypsin-EDTA, opti-MEM, Dulbecco's Phosphate-Buffered Saline (DPBS).

5.2. Murine Mesenchymal stem cell derived Extracellular Vesicles (mMSC-EVs)

Two batches of EVs derived from murine Mesenchymal Stem Cells (mMSC) were used. mMSC-EV#1 was obtained from Everzom (Paris, France, products #230801-G5 and #230608-G12). Briefly, EVs from Murine C3H/10T1/2, Clone 8 (ATCC® CCL-226™) cells were produced and isolated using Everzom's optimized 3D biomanufacturing and isolation processes, followed by an additional purification step with Size Exclusion Chromatography (SEC; Captocore 700). The column volume was adapted to the protein concentration measured after Tangential Flow Filtration (TFF). A 1:10 addition of 250mM trehalose (for a final concentration of 25mM) was done before freezing the sample in cryotubes. mMCS-EV#2 were produced following a well-established protocol in our laboratory[55]. The final EV pellet was resuspended in DPBS buffer containing 25mM of trehalose and stored at -80°C.

5.3. Synthesis of HRP conjugates

5.3.1. Synthesis of Lipid-PEG-HRP

Stock solutions of Lipid-PEG-SH (structures and conjugation process are described in Supplementary Figure 1A&B) were obtained by dissolving 20g/l of powder in ultrapure water. EZ-Link™ Maleimide Activated Horseradish Peroxidase (mal-HRP) was rehydrated in H_2O for a final concentration of 2g/l before addition of 20 molar equivalents of Lipid-PEG-SH (Lipid-Anchor abbreviated as LA). Depending on the LA MW and the final volume needed, 45µl to 122µl of lipid-PEG-SH were added to 500µl to 1000µl of mal-HRP. Water was added according to the volume of added LA

to obtain identical final concentration is all mixes, equal to $7.8x10^{-4}$M of Lipid-PEG-SH (1.4 to 4.5g/l according to the MW of the LA) with $3.9x10^{-5}$M (1.6g/l) of mal-HRP.

The mix was then incubated at 37°C overnight under gentle agitation to enable the Michael addition reaction between the thiol function of Lipid-PEG-SH and the maleimide function of mal-HRP (maleimide/HRP ratio equal to 3 mole/mole according to the provider). A dialysis step (Slide-A-Lyzer® Dialysis Cassette 20000 MWCO, 0.5ml, Thermo Fisher Scientific®) was performed against DPBS under gentle agitation to eliminate unconjugated Lipid-PEG-SH. Dialysis buffer was frequently changed (2h at RT, 2h at 30°C and finally 20h at 4°C). MW of DSPE-PEG_{1000}-HRP, DSPE-PEG_{2000}-HRP, DSPE-PEG_{5000}-HRP and CLS-PEG_{2000}-HRP were observed using HPLC-MS (Supplementary Figure 1C) and mass gains of respectively 1392g/mol, 2362g/mol, 4815g/mol and 2154g/mol as compared to unconjugated HRP were measured. Enzymatic assay revealed that Lipid-PEG-HRP retained 80-95% of its biological activity regardless of the type of Lipid-PEG after conjugation and dialysis (Supplementary Figure 1D).

5.3.2. Synthesis of fluorescent Lipid-PEG-HRP-A488

Alexa-Fluor 488 was conjugated with Lipid-PEG-HRP to obtain Lipid-PEG-HRP-A488 for single-particles analysis and cell internalization microscopic observations using Alexa Fluor® 488 Microscale Protein Labeling Kit (Thermo Fisher Scientific®) following manufacturer's protocol. Fluorescent conjugates were purified using Zeba™ Dye and Biotin Removal Spin Columns (Thermo Fisher Scientific®) and 50mM of Tris-HCl were added to quench the reactivity of residual dye and avoid further artifactual conjugation of the dye with EV proteins.

5.4. Lipid-PEG-HRP and EVs association

5.10^{10} EV/ml (assessed by NanoTracking Analysis, NTA) were mixed with different final concentrations of Lipid-PEG-HRP (from 0.5mg/ml to 75mg/ml). Depending on the requirements of the experiment, volumes of preparation were comprised between 50µl and 1ml. Samples were incubated overnight at 25°C or 37°C depending on the experiment, under gentle agitation.

5.5. Purification of EV~Lipid-PEG-HRP

SEC separation was used for all samples except in indicated microscopy experiments (Figure 8). Columns were packed following Tulkens *et al.*[56] protocol. Briefly, 6ml of sepharose CL-2B were poured inside a syringe body (10ml Luer slip, Fisherbrand™) obstructed with a quarter of filter (20µm Nylon Net 25mm hydrophilic, Sigma Aldrich®). After sedimentation of sepharose, one Column Volume

(CV) was equal to 4ml and each column was used once. The resin settled overnight at 4°C before use and was washed with 3 CV of DPBS. 50µl of EV/HRP mixture at 5.10^{10} EV/ml were diluted 11-fold in DPBS and 500µl of sample were deposited on the top of the column. 500µl elution fractions were collected and analyzed (NTA, enzymatic activity). Depending on the experiment and the purity level needed, only the 4th fraction or the combination of 3rd, 4th and 5th fractions was collected.

Samples used for microscopy observations in Figure 8 were purified using tangential ultrafiltration with Amicon® 100kDa 0.5ml (Merck Millipore®) in order to avoid the dilution resulting from SEC. 500µl of samples previously diluted by 10 in DPBS were deposited in Amicon® filter before centrifugation at 2000g during 15min at 4°C (Centrifuge 5804 R, Eppendorf®). Then, retentates were diluted by 10 in DPBS once again to obtain 500µl before a second identical centrifugation. Final EV-containing retentates were analyzed using NTA and TMB enzymatic assay.

5.6. Characterization

5.6.1. NanoTracking Analysis (NTA)

EVs were analyzed with a NanoSight NS300 (Malvern Panalytical Instruments, UK). Samples were diluted with particle-free DPBS in order to obtain a concentration range between 1.10^8 and 5.10^8 particles/ml. Measurements were performed with a 405nm and a 488nm laser. Data were collected using the NanoSight NTA 3.4 software following a tailored script: temperature was set at 25°C, syringe pump at 40 arbitrary units and 5 videos of 60s were recorded with a camera level set to 15 and analyzed with a detection threshold set to 5. All groups of compared data were measured and analyzed using identical conditions.

Zetaview® (Particle Metrix, USA) was used for Zeta potential (ZP) and particle fluorescence measurements. For ZP measurements, 2-cycles measurements on 2 positions (SL1 and SL2) using a 488nm laser were used with a sensitivity set at 80 and a shutter at 100. Samples were diluted to obtain a final EV concentration equal to 5.10^7 EV/ml in 1:10 DPBS (1.5mM). Sensed conductivity was equal to 145µS/cm. For particle fluorescence measurement, two successive measurements were done in fluorescent and scatter mode. Fluorescence measurements were performed with a sensitivity of 90 and a shutter of 50 using a 488nm laser and a 500nm filter, while scatter measurements were carried out with a sensitivity of 80 and a shutter of 100 without filter. Concentration correction factor was calculated following manufacturer's guidelines by using reference fluorescent beads YG-488 and was equal to 1.1. Data were analyzed using Software ZetaView (8.05.16 SP3 version).

5.6.2. HPLC-MS experiments

ElectroSpray Ionization Mass Spectrometry (ESI/MS) and MS/MS analyses were performed on a Synapt G2-S instrument equipped with Ultra Performance Liquid Chromatography (Waters Corporation, UK). For the separation, a gradient with H_2O containing 0.1% of formic acid (FA) as eluent A and acetonitrile containing 0.1% of FA as eluent B was applied as follow: from 95% A to 70% in 8min and from 70% until 50% between 8 and 25min before going back to 95% A in a total run of 35min, at a flow rate of 0.45ml/min on a polyphenyl column (BioResolve, 150x2.1mm, 2.7µm particle size), designed for intact proteins and antibodies analysis. UV detection was done at 220nm and 280nm. Mass spectrum acquisition was performed with a mass range of m/z 800-5000, a scan time of 0.5s in a positive ion mode with capillary voltage 3kV, 40°C and 350°C for the source and desolvation temperatures, respectively. MassLynx software was used for data acquisition and processing, with the MaxEnt1 module for the deconvolution process.

5.6.3. Enzymatic assay and determination of EV-associated HRP amount

50µl of sample were added to 50µl of Tetramethylbenzidine (TMB) and incubated 30min at RT in 96-well plate (Nunc MaxiSorp™, Invitrogen™). Then, 50µl of sulfuric acid (2M) were added to stop reaction. Absorbance at 450nm was then measured to quantify the HRP activity using a MultiScan Go (Thermo Fisher Scientific™). Standard curves were made using pre-SEC samples to assess HRP concentration in post-SEC samples. Standard curves and assessed samples were always processed at the same time (usually after 30min of incubation). HRP standard curves were typically linear in the range of 0-2ng/ml.

5.6.4. MACSPlex assay

EV surface epitopes determination was performed using the MACSPlex Exosome Kit mouse (Miltenyi Biotec®). The test was done according to the manufacturer protocol. Briefly, 1.10^9 EVs were diluted in 120µl MACSPlex Buffer. MACSPlex Exosome Capture Beads and Detection Reagent CD9, CD63 and CD81 were then added to the EV suspension and incubated for 1h at RT under gentle agitation (450rpm) protected from light. After washing steps, samples were analyzed using a BD Accuri C6 (BD Biosciences, USA). For each sample, the obtained median fluorescence intensity (MFI) of 37 exosomal surface epitopes and two isotype controls were subtracted from the corresponding MFI of the blank. This blank was the EVs buffer diluted in the same way as EV samples, mixed with capture beads and detection reagent without EVs.

5.6.5. NanoFlowCytometry (nanoFCM)

NanoFCM™ was used in 40-200nm range mode. Alexa-Fluor 647 anti-mouse IgG1 (isotype control), APC anti-mouse CD63 Alexa-Fluor 647, APC anti-mouse CD9 Alexa-Fluor 647 and APC anti-mouse/rat CD81 Alexa-Fluor 647 (Biolegend) were diluted at 1:50000 before incubation with sample diluted at 5.10^8 EV/ml at 4°C overnight (ON).

5.6.6. Cryo-Transmission Electron Microscopy (cryo-TEM) imaging

Samples were imaged using cryo-TEM. Carbon film coated EM grids (Ted Pella Inc.) were glow-discharged at 30mA, for 30s (Pelco easiGlow, Ted Pella Inc.). 4µl of each sample solution was applied to the carbon-coated side of the TEM grid, blotted for 10s, before plunge-freezing in liquid ethane using the Vitrobot Mark MkIII (FEI). Vitrified samples were then imaged in a Glacios cryo-transmission electron microscope (ThermoFisher) equipped with a K3 direct electron detector, SerialEM software (D. Mastronarde, Boulder Lab) was used in acquisition.

5.6.7. Super-resolution microscopy imaging

Single molecule localization microscopy was performed using an ONI Nanoimager (ONI Bio). Native EV samples were incubated with CD9 Alexa-Fluor 488, CD63 Alexa-Fluor 568, and CD81 Alexa-Fluor 647 monoclonal antibodies from the EV Profiler kit (ONI Bio). Processed EV samples (associated with Lipid-PEG-HRP-A488 obtained as described in 5.3.2. section, and controls) were incubated with CD9 Alexa-Fluor 647 (Clone MZ3, BioLegend) and Vybrant DiI (Invitrogen, Thermo Fisher) overnight at 4°C on a plate shaker. 10µl of each fluorescent antibody or dye were added along with 10µl blocking solution B1 from the EV Profiler kit (ONI Bio) per 150µl sample. Unbound antibody and dye were removed after overnight incubation at the same time than free Lipid-PEG-HRP using SEC (70nm qEV, IZON). 10µl droplet was added between a 1mm TOMO adhesion glass slide (Avantor) and a #1 glass cover slip (Corning) for immediate imaging. Briefly, the instrument was calibrated for direct stochastic optical reconstruction microscopy with bead calibration (ONI Bio) slide using NimOS version 1.19.7. 3-color super resolution microscopy was then performed with 500 frames taken per channel. Laser powers were adjusted according to company standard operating procedures. Raw image files were uploaded to the cloud software CODI via CODI Desktop Uploader version 0.30.0. Image analysis was performed on CODI. Briefly, drift correction, filtering, clustering, and counting algorithms were performed using the predefined “EV Profiling” workflow.

5.7. Stability assessment of EV / Lipid-PEG-HRP association

Stability of the association was assessed under different conditions of storage. Samples were diluted at 1:11 in DPBS or DPBS supplemented with FBS (1:50) before incubation at 4°C or 37°C during 2h or overnight. A condition was also carried out with a freeze/thaw (F/T) at -80°C in DPBS. Then, free HRP was removed using SEC separation and samples were analyzed using TMB enzymatic assay and NTA measurements.

5.8. Cell internalization experiments

5.8.1. Quantitative cell lysis experiments

1.10^5 PANC-1 (ATCC, CRL-1469 ™), SKBR3 (ATCC, HTB-30™) and A509 (ATCC, CCL-185™) cells in 1ml of DMEM supplemented with 10% FBS, 2mM L-glutamine, 100U/ml penicillin and 100µg/ml streptomycin were plated in 24-well plate and incubated at 37°C and 5% CO_2 prior to cell internalization experiments. After 24h, medium was discarded and replaced by samples to be tested diluted in fresh identical medium for a total volume of 400µl. Cells and samples were then incubated at 37°C with different amounts of HRP (from 1ng to 15ng of HRP/well), for different time periods (2h, 4h or 24h) depending on the experiment. Sample-containing medium was afterwards removed and cells were washed with cold DPBS 3 times before addition of 200µl of M-PER™ supplemented with protease inhibitor and incubated 5min at RT under gentle shaking. To ensure optimal lysis, cells were then pipetted in the well and collected in microtubes before 10s vortex. Lysates were finally centrifuged during 15min at 4°C and 14000g to keep only the supernatant. HRP activity was measured with TMB following protocol described in 5.6.3. except that all dilutions and standard curves were diluted in lysis buffer instead of DPBS to avoid any bias on the peroxidase activity from surfactants present in lysate. Blank was done with untreated cells control lysate.

5.8.2. Microscopy observations and quantifications

For these experiments, samples were purified by ultrafiltration (UF) instead of SEC to maximize their concentration in order to obtain good fluorescence signal-to-noise ratio. After UF, EV / unconjugated HRP-A488 and EV~CLS-PEG_{2000}-HRP-A488 samples were at 357ng/ml and 941ng/ml, respectively. EVs samples were at 5.10^9p/ml. Identical concentrations of unconjugated HRP-A488 and CLS-PEG_{2000}-HRP-A488 were used for controls without EVs. A549 cells were seeded at 17500 cells per well in 8-well Nunc™ Lab-Tek™ II Chamber Slide™ plates (ThermoFischer) and incubated during 24h at 37 °C in a humidified 5% v/v CO_2 atmosphere. Then, 150µl of samples diluted with 150µl of DMEM supplemented with 10% FBS, 2mM L-glutamine, 100U/ml penicillin and 100µg/ml streptomycin were

added and incubated during 5h with cells. Cells were washed with DPBS, labeled with CellMask™ (1:1000 dilution in fresh medium) and incubated for 30min. Finally, cells were fixed in DPBS with 4% formaldehyde (36% w/w) during 10min at room temperature and washed with DPBS. DAPI (1µg/ml in DPBS) was added and left for 5min before washing. Slide was mounted with Prolong™ mounting medium for microscopy observations.

For the panel (Figure 8A to 8E), images were acquired using a full-field epifluorescence microscope Nikon Ti2 (Nikon Instrument Inc®), with a CMOS back-illuminated Prime95B (1200*1200 pixels, 11µm pixel, Teledyne Photometrics®) camera, Lumencor® system as a source of illumination and 40X objective (oil, 1.3 numerical aperture). Images were treated with Fiji (ImageJ) software with identical adjustment of brightness and contrast. The set parameters minimum/maximum displayed values were equal to 3000/62000 for HRP-488, -140/17500 for CellMask™ and 6800/34500 for DAPI staining.

For quantitative analysis, images were acquired on the same samples using a spinning-disk confocal microscope with a Yokogawa CSU-W1 spinning head (Yokogawa Electric Corporation®) on a sCMOS back-illuminated Prime95B (1200*1200, 11µm pixel) camera and Nikon 60X objective (Plan Apo, 1.4 numerical aperture). Images were taken with a Z-step of 210nm using an Oxxius® lasers (excitation at 488nm and 561nm). Image processing for quantitative analysis was performed using Fiji. Cells were segmented into a binary mask using the random-forest pixel-classifier algorithm (Labkit ImageJ plugin) to attribute a class ("inside cell" or "background") to every pixel. Spot detection was done by applying a Laplacian of Gaussian filter before local minima detection (using FeatureJ Log filter and MorphoLibJ local minima detector) to extract a 3D point per spot. List of coordinates generated based on CellMask™ were used to differentiate cells from background in order to count HRP-A488 fluorescent spots inside cells. This number of internalized fluorescent spots was normalized per the total number of intracellular voxels in order to normalize the difference in cell number per image.

5.9. Statistical analysis

RStudio version 1.4.1717 (2009-2021 RStudio, PBC®) was used for *post hoc* statistical analysis. Unilateral or two-tailed Welch tests were used depending on the null hypothesis as indicated in figure legends.

Acknowledgements

The authors gratefully acknowledge the French National Research Agency (ANR-20-CE09-0011-01), the imaging facility MRI, member of the France-BioImaging national infrastructure supported by the French National Research Agency (ANR-10-INBS-04, «Investments for the future»), IVETh Core

Facility, and specifically Kelly Aubertin, Sarah Razafindrakoto and Christopher Ribes for fruitful discussions and for performing the NanoFCM analyses. IVETh is supported by the IdEx Université Paris Cité, ANR-18-IDEX-0001, by the Region Ile de France under the convention SESAME 2019 – IVETh (EX047011) and via the DIM BioConvS, by the Région Ile de France and Banque pour l'Investissement (BPI) under the convention Accompagnement et transformation des filières projet de recherche et développement N° DOS0154423/00 & DOS0154424/00, DOS0154426/00 & DOS0154427/00, and Agence Nationale de la Recherche through the program France 2030 "Integrateur biotherapie-bioproduction" (ANR-22-AIBB-0002). Funding for work by S. Emerson was provided by the California Institute of Regenerative Medicine Bridges program (EDUC2-12620).

Declaration of Interest Statement: The authors report no conflict of interest.

AUTHOR CONTRIBUTIONS

Antonin Marquant: Conceptualization (lead); Investigation (lead); Methodology (lead); Data Curation; Formal analysis (lead); Validation; Visualization; Writing—original draft (lead); Writing—review & editing. **Jade Berthelot**: Conceptualization; Investigation; Methodology; Validation, Vizualization. **Claudia Bich**: Conceptualization; Investigation; Methodology; Validation, Vizualization. **Zeineb Ibn Elfekih**: Investigation; Methodology; Validation; Vizualization. **Laurianne Simon**: Conceptualization (supporting); Investigation. **Baptiste Robin**: Conceptualization (supporting); Investigation. **Joël Chopineau**: Conceptualization (supporting); Resources. **David Tianpei Wang**: Investigation; Methodology; Formal analysis; Data curation; Validation; Vizualization. **Samuel J Emerson**: Investigation; Data Curation; Formal analysis. **Aijun Wang**: Conceptualization; Resources. **Clément Benedetti**: Investigation; Methodology; Formal analysis; Data curation; Validation; Vizualization. **Simon Langlois**: Investigation; Methodology; Formal analysis; Data curation; Validation; Vizualization. **Laurence Guglielmi**: Conceptualization (supporting); Methodology; Resources. **Pierre Martineau**: Conceptualization (supporting); Methodology; Resources. **Anne Aubert-Pouëssel**: Conceptualization (lead); Supervision (co-lead); Visualization; Writing—original draft; Writing—review & editing (co-lead). **Marie Morille**: Conceptualization (lead); Supervision (lead); Validation; Vizualization; Funding acquisition; Project administration; Resources; Writing—original draft preparation; Writing—review & editing (lead). **All authors** provided critical feedback and helped shape the research, analysis and manuscript.

References

1. Tanaka, T. & Rabbitts, T. H. Interfering with protein-protein interactions: Potential for cancer therapy. *Cell Cycle* **7**, 1569–1574 (2008).

2. Gulfidan, G., Turanli, B., Beklen, H., Sinha, R. & Arga, K. Y. Pan-cancer mapping of differential protein-protein interactions. *Sci. Rep.* **10**, 3272 (2020).

3. Ivanov, A. A., Khuri, F. R. & Fu, H. Targeting protein–protein interactions as an anticancer strategy. *Trends Pharmacol. Sci.* **34**, 393–400 (2013).

4. Maes, M., Loyter, A. & Friedler, A. Peptides that inhibit HIV-1 integrase by blocking its protein–protein interactions. *FEBS J.* **279**, 2795–2809 (2012).

5. Naren, A. P., Quick, M. W., Collawn, J. F., Nelson, D. J. & Kirk, K. L. Syntaxin 1A inhibits CFTR chloride channels by means of domain-specific protein–protein interactions. *Proc. Natl. Acad. Sci.* **95**, 10972–10977 (1998).

6. Poluri, K. M., Gulati, K., Tripathi, D. K. & Nagar, N. Protein–Protein Interactions in Immune Disorders and Inflammation. in *Protein-Protein Interactions: Pathophysiological and Therapeutic Aspects: Volume II* (eds. Poluri, K. M., Gulati, K., Tripathi, D. K. & Nagar, N.) 171–206 (Springer Nature, Singapore, 2023). doi:10.1007/978-981-99-2423-3_4.

7. Andrews, M. D. *et al.* Discovery of an Oral, Rule of 5 Compliant, Interleukin 17A Protein–Protein Interaction Modulator for the Potential Treatment of Psoriasis and Other Inflammatory Diseases. *J. Med. Chem.* **65**, 8828–8842 (2022).

8. Gurevich, E. V. & Gurevich, V. V. Therapeutic Potential of Small Molecules and Engineered Proteins. in *Arrestins - Pharmacology and Therapeutic Potential* (ed. Gurevich, V. V.) 1–12 (Springer, Berlin, Heidelberg, 2014). doi:10.1007/978-3-642-41199-1_1.

9. Lu, R.-M. *et al.* Development of therapeutic antibodies for the treatment of diseases. *J. Biomed. Sci.* **27**, 1 (2020).

10. Ebrahimi, S. B. & Samanta, D. Engineering protein-based therapeutics through structural and chemical design. *Nat. Commun.* **14**, 2411 (2023).

11. Yu, M., Wu, J., Shi, J. & Farokhzad, O. C. Nanotechnology for protein delivery: Overview and perspectives. *J. Controlled Release* **240**, 24–37 (2016).

12. Le Saux, S. *et al.* Nanotechnologies for Intracellular Protein Delivery: Recent Progress in Inorganic and Organic Nanocarriers. *Adv. Ther.* **4**, 2100009 (2021).

13. Strohl, W. R. Current progress in innovative engineered antibodies. *Protein Cell* **9**, 86–120 (2018).

14. Slastnikova, T. A., Ulasov, A. V., Rosenkranz, A. A. & Sobolev, A. S. Targeted Intracellular Delivery of Antibodies: The State of the Art. *Front. Pharmacol.* **9**, 1208 (2018).

15. Le Saux, S. *et al.* Interest of extracellular vesicles in regards to lipid nanoparticle based systems for intracellular protein delivery. *Adv. Drug Deliv. Rev.* **176**, 113837 (2021).

16. Herrmann, I. K., Wood, M. J. A. & Fuhrmann, G. Extracellular vesicles as a next-generation drug delivery platform. *Nat. Nanotechnol.* **16**, 748–759 (2021).

17. Mizrak, A. *et al.* Genetically Engineered Microvesicles Carrying Suicide mRNA/Protein Inhibit Schwannoma Tumor Growth. *Mol. Ther.* **21**, 101–108 (2013).

18. Haney, M. J. *et al.* TPP1 Delivery to Lysosomes with Extracellular Vesicles and their Enhanced Brain Distribution in the Animal Model of Batten Disease. *Adv. Healthc. Mater.* **8**, e1801271 (2019).

19. Heath, N. *et al.* Endosomal escape enhancing compounds facilitate functional delivery of extracellular vesicle cargo. *Nanomed.* **14**, 2799–2814 (2019).

20. Zhang, X. *et al.* Programmable Extracellular Vesicles for Macromolecule Delivery and Genome Modifications. *Dev. Cell* **55**, 784-801.e9 (2020).

21. Lainšček, D. *et al.* Delivery of an Artificial Transcription Regulator dCas9-VPR by Extracellular Vesicles for Therapeutic Gene Activation. *ACS Synth. Biol.* **7**, 2715–2725 (2018).

22. Ilahibaks, N. F. *et al.* TOP-EVs: Technology of Protein delivery through Extracellular Vesicles is a versatile platform for intracellular protein delivery. *J. Controlled Release* **355**, 579–592 (2023).

23. Wang, Z. *et al.* Exosomes decorated with a recombinant SARS-CoV-2 receptor-binding domain as an inhalable COVID-19 vaccine. *Nat. Biomed. Eng.* **6**, 791–805 (2022).

24. Silva, A. M. *et al.* Quantification of protein cargo loading into engineered extracellular vesicles at single-vesicle and single-molecule resolution. *J. Extracell. Vesicles* **10**, e12130 (2021).

25. Yim, N. *et al.* Exosome engineering for efficient intracellular delivery of soluble proteins using optically reversible protein–protein interaction module. *Nat. Commun.* **7**, 12277 (2016).

26. Wang, Q. *et al.* ARMMs as a versatile platform for intracellular delivery of macromolecules. *Nat. Commun.* **9**, 960 (2018).

27. Xie, F. *et al.* Engineering Extracellular Vesicles Enriched with Palmitoylated ACE2 as COVID-19 Therapy. *Adv. Mater.* **33**, 2103471 (2021).

28. Uppu, D. S. *et al.* Glycolipid-Anchored Proteins on Bioengineered Extracellular Vesicles for Lipopolysaccharide Neutralization. *ACS Appl. Mater. Interfaces* **13**, 29313–29324 (2021).

29. Whitley, J. A. *et al.* Encapsulating Cas9 into extracellular vesicles by protein myristoylation. *J. Extracell. Vesicles* **11**, (2022).

30. Lamichhane, T. N., Raiker, R. S. & Jay, S. M. Exogenous DNA Loading into Extracellular Vesicles via Electroporation is Size-Dependent and Enables Limited Gene Delivery. *Mol. Pharm.* **12**, 3650–3657 (2015).

31. Corso, G. *et al.* Systematic characterization of extracellular vesicle sorting domains and quantification at the single molecule – single vesicle level by fluorescence correlation spectroscopy and single particle imaging. *J. Extracell. Vesicles* **8**, 1663043 (2019).

32. Ivanova, A. *et al.* Creating Designer Engineered Extracellular Vesicles for Diverse Ligand Display, Target Recognition, and Controlled Protein Loading and Delivery. *Adv. Sci.* **10**, 2304389 (2023).

33. Rankin-Turner, S. *et al.* A call for the standardised reporting of factors affecting the exogenous loading of extracellular vesicles with therapeutic cargos. *Adv. Drug Deliv. Rev.* **173**, 479–491 (2021).

34. Choi, E. S., Song, J., Kang, Y. Y. & Mok, H. Mannose-Modified Serum Exosomes for the Elevated Uptake to Murine Dendritic Cells and Lymphatic Accumulation. *Macromol. Biosci.* **19**, 1900042 (2019).

35. Pitchaimani, A. *et al.* Compartmentalized drug localization studies in extracellular vesicles for anticancer therapy. *Nanoscale Adv.* **5**, 6830–6836 (2023).

36. Didiot, M.-C. *et al.* Exosome-mediated Delivery of Hydrophobically Modified siRNA for Huntingtin mRNA Silencing. *Mol. Ther.* **24**, 1836–1847 (2016).

37. Haraszti, R. A. *et al.* Optimized Cholesterol-siRNA Chemistry Improves Productive Loading onto Extracellular Vesicles. *Mol. Ther.* **26**, 1973–1982 (2018).

38. Stremersch, S. *et al.* Comparing exosome-like vesicles with liposomes for the functional cellular delivery of small RNAs. *J. Controlled Release* **232**, 51–61 (2016).

39. Zhang, H. *et al.* Exosome-mediated targeted delivery of miR-210 for angiogenic therapy after cerebral ischemia in mice. *J. Nanobiotechnology* **17**, 29 (2019).

40. Gong, C. *et al.* Functional exosome-mediated co-delivery of doxorubicin and hydrophobically modified microRNA 159 for triple-negative breast cancer therapy. *J. Nanobiotechnology* **17**, 93 (2019).

41. Jing, B. *et al.* Extracellular vesicles-based pre-targeting strategy enables multi-modal imaging of orthotopic colon cancer and image-guided surgery. *J. Nanobiotechnology* **19**, 151 (2021).

42. Zheng, W. *et al.* Surface display of functional moieties on extracellular vesicles using lipid anchors. *J. Controlled Release* **357**, 630–640 (2023).

43. Kooijmans, S. A. A. *et al.* PEGylated and targeted extracellular vesicles display enhanced cell specificity and circulation time. *J. Controlled Release* **224**, 77–85 (2016).

44. Wiklander, O. P. B. *et al.* Systematic Methodological Evaluation of a Multiplex Bead-Based Flow Cytometry Assay for Detection of Extracellular Vesicle Surface Signatures. *Front. Immunol.* **9**, (2018).

45. Tréton, G. *et al.* Quantitative and functional characterisation of extracellular vesicles after passive loading with hydrophobic or cholesterol-tagged small molecules. *J. Controlled Release* **361**, 694–716 (2023).

46. Aumiller, W. M. Jr., Davis, B. W., Hatzakis, E. & Keating, C. D. Interactions of Macromolecular Crowding Agents and Cosolutes with Small-Molecule Substrates: Effect on Horseradish Peroxidase Activity with Two Different Substrates. *J. Phys. Chem. B* **118**, 10624–10632 (2014).

47. Mitrut, R. E. *et al.* HaloTag display enables quantitative single-particle characterisation and functionalisation of engineered extracellular vesicles. *J. Extracell. Vesicles* **13**, e12469 (2024).

48. Chen, C. *et al.* Active cargo loading into extracellular vesicles: Highlights the heterogeneous encapsulation behaviour. *J. Extracell. Vesicles* **10**, e12163 (2021).

49. Alwarawrah, M., Dai, J. & Huang, J. A Molecular View of the Cholesterol Condensing Effect in DOPC Lipid Bilayers. *J. Phys. Chem. B* **114**, 7516–7523 (2010).

50. Skotland, T., Sagini, K., Sandvig, K. & Llorente, A. An emerging focus on lipids in extracellular vesicles. *Adv. Drug Deliv. Rev.* **159**, 308–321 (2020).

51. Biscans, A. *et al.* Hydrophobicity of Lipid-Conjugated siRNAs Predicts Productive Loading to Small Extracellular Vesicles. *Mol. Ther.* **26**, 1520–1528 (2018).

52. Erdőssy, J., Kassa, E., Farkas, A. & Horváth, V. Enzymatic digestion as a tool for removing proteinaceous templates from molecularly imprinted polymers. *Anal. Methods* **9**, 4496–4503 (2017).

53. Hagey, D. W. *et al.* The cellular response to extracellular vesicles is dependent on their cell source and dose. *Sci. Adv.* **9**, eadh1168 (2023).

54. Vonarbourg, A., Passirani, C., Saulnier, P. & Benoit, J.-P. Parameters influencing the stealthiness of colloidal drug delivery systems. *Biomaterials* **27**, 4356–4373 (2006).

55. Le Saux, S. *et al.* Post-production modifications of murine mesenchymal stem cell (mMSC) derived extracellular vesicles (EVs) and impact on their cellular interaction. *Biomaterials* **231**, 119675 (2020).

56. Tulkens, J., De Wever, O. & Hendrix, A. Analyzing bacterial extracellular vesicles in human body fluids by orthogonal biophysical separation and biochemical characterization. *Nat. Protoc.* **15**, 40–67 (2020).